ANALYTICAL APPLICATIONS OF CONVERSION ELECTRON MÖSSBAUER SPECTROMETRY (CEMS)

Yusuke Ujihira

Department of Industrial Chemistry
Faculty of Engineering, The University of Tokyo,
7-3-1, Hongo, Bunkyo-ku, Tokyo, 113, Japan

CONTENTS

		Page
SUN	(MARY	127
1.	INTRODUCTION	127
2.	SCHEMATIC ARRANGEMENT OF MÖSSBAUER SPECTROMETER	128
3.	RELAXATION PROCESS OF EXCITED ⁵⁷ Fe NUCLEUS	128
4.	DETECTORS FOR REEMITTED RADIATIONS	130
	4.1. Detection of Reemitted γ Rays	130
	4.2. Detection of Reemitted X Ray	131
	4.3. Detectors for Conversion and Auger Electrons	134
5.	DEPTH SELECTIVE OBSERVATION OF SURFACES BY CEMS	134
6.	MÖSSBAUER PARAMETERS	138
	6.1. Isomer Shift (I.S. or δ)	138
	6.2. Magnetic Splitting (Represented in Terms of Internal	
	Magnetic Field H _{int})	138
	6.3. Quadrupole Splitting (Q.S. or Δ)	144
7.	APPLICATIONS	146
	7.1. Orientation of the Magnetic Field (Axis of Quantization))
	of Iron and Steel at the Surface	146
	7.2. Characterization of Surface Products on Oxidized	
	Steels	147
	7.3. Corrosion Study of Steels in Atmospheres Containing	
	$HCl, SO_2 \text{ or } H_2S$	153
	7.4. Analyses of Phosphate and Oxalate Coatings of Steels	154
	7.5. Analysis of Hardened Steel Surfaces	160
	7.6. Characterization of Intermetallic Compounds Formed	
	at the Interface of Coated Metal and Steel	166

7.7 STUDY OF PHASE TRANSFORMATION	169
7.8 STUDY OF CRYSTALLIZATION OF AMORPHOUS IRON	171
7.9 CEMS FOR 119 Sn AND 181 Ta	171
ACKNOWLEDGEMENT	175
REFERENCES	175

SUMMARY

Recent developments of conversion electron Mossbauer spectrometry (CEMS), a promising new technique of surface analysis, are reviewed. Its applications to the characterization of corrosion products or phosphated coatings produced on steel, to the layer-by-layer analysis of the hardened steel surface, to the estimation of intermetallic compounds formed between Iron-Zinc and Iron-Tin interfaces, and to studies of surface deposition of iron compounds by the crystallization of amorphous iron are presented.

* * *

Some parts were presented as a review talk at the panel discussion of the International Conference on the Application of the Mossbauer Effect (December, 1981, Jaipur, India). Proceedings of the Indian National Science Academy — Physical Science Special Volume, pp. 166-170 (1982).

1. INTRODUCTION

Mossbauer spectrometry, based on the resonant absorption of γ rays by the nucleus, has been developed as a new instrumental technique for studies of solid state physics, inorganic and analytical chemistry, and metallurgy. Recently its applications have spread to the field of polymer science, geology, archaeology, art and biology. Several monographs and reviews have been published /1, 2, 3, 4, 5/. The spectra provide us with valuable scientific information through Mossbauer parameters — isomer shift (I.S.), quadrupole splitting (Q.S.), recoilless fraction (f), line width ($\Delta\Gamma$), magnetic splitting by internal magnetic field (H_{int}), etc. — because these parameters reflect the physico-chemical environment around the Mossbauer nucleus present in solid samples.

In particular, Mossbauer spectrometry has been applied to the chemical state analysis of iron (57 Fe) and tin (119 Sn) compounds from the viewpoint of experimental feasibility and practical importance of these compounds. Other elements, to which Mossbauer spectrometry is applied without many difficulties, are Ru (99 Ru), Sb (121 Sb), Te (125 Te), I (127 I, 129 I), Sm (149 Sm), Eu (151 Eu), Gd (155 Gd), Dy (161 Dy), Tm (169 Tm), Yb (170 Yb), Ir (193 Ir), Au (197 Au) and Np (237 Np).

Mössbauer spectrometry by detecting conversion electrons reemitted from the excited nucleus have been reported for ⁵⁷Fe, ¹¹⁹Sn, ¹⁵¹Eu, ¹⁶⁹Tm and ¹⁸¹Ta due to intrinsic and experimental restrictions /6, 7, 8, 9, 10, 11/.

In this article, I describe the outline of conversion electron Mössbauer spectrometry and briefly review its application to the analyses of the chemical states of iron and tin formed in the surface layers of chemically treated steels and tin, respectively. The advantages of CEMS as a tool for the surface analysis are

- 1. its depth resolution, several 10 nm;
- 2. its potential to reveal the chemical states of iron and tin in solid surfaces.

These features increase the versatility of CEMS for the surface analysis of industrial materials as well as to studies of the oxidation and corrosion of steels and to the surface characterization of minerals, ceramics and ion implanted materials /12, 13/.

2. SCHEMATIC ARRANGEMENT OF A MÖSSBAUER SPECTROMETER

Since the discovery of the Mössbauer effect in 1957 /14/, most Mössbauer spectrometers have been designed and operated by transmission geometry detecting transmitted γ rays by a scintillation counter of 0.5 mm thick NaI (Tl) or a proportional counter as shown in Fig. 1-a. But, during the past 5 years, considerable development has been achieved both in theory and instrumentation for measuring Mössbauer spectra by back-scatter geometry, detecting reemitted γ rays, X rays or electrons (Fig. 1-b and 1-c). The arrangement permits the observation of the Mössbauer spectrum of solid surfaces and scattering Mössbauer spectrometry has been developed as an efficient technique for characterising the surface of chemically and metallurgically treated steel and tin.

3. RELAXATION PROCESS OF EXCITED 57Fe NUCLEUS

The Mössbauer nucleus becomes excited after resonant absorption of a γ ray. The ⁵⁷Fe nucleus absorbs the 14.4 keV γ ray radiated by the decay of ⁵⁷Co and gets excited. The excited state of ⁵⁷Fe is relaxed by energy degradation following the process shown in Fig. 2. 10% of the excited ⁵⁷Fe reemits the 14.4 keV γ ray, while 89%

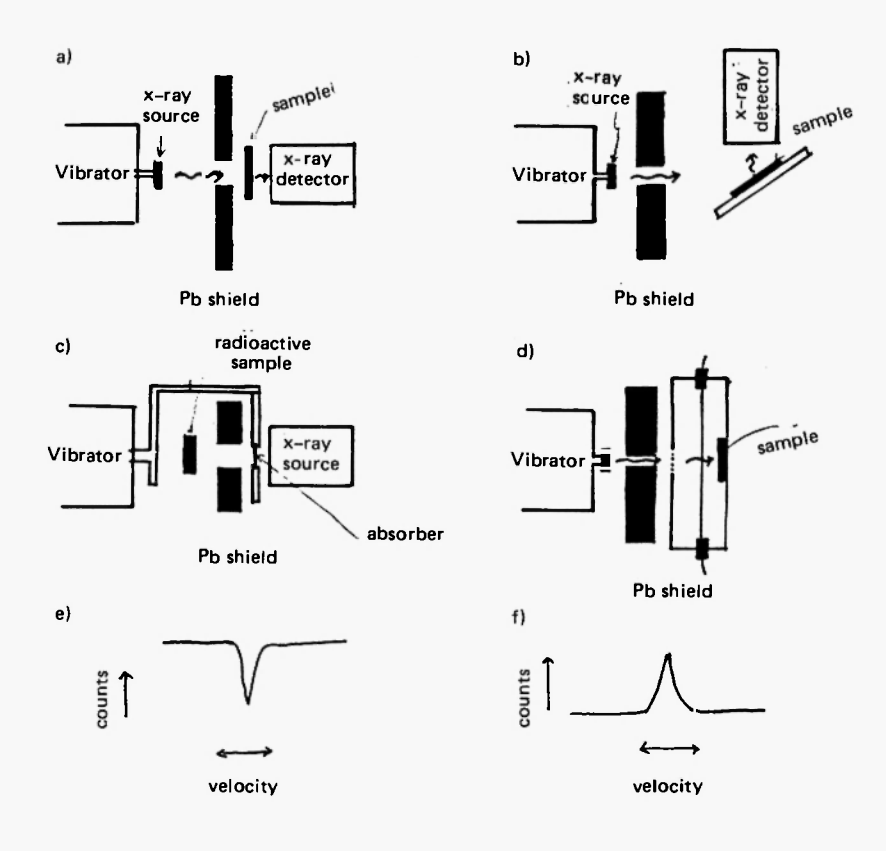


Fig. 1. Geometrical arrangements and observed spectra (cited from ref. [12])

- (a) Transmission Mössbauer spectrometry (TMS)
- (b) Scattered γ ray and re-emitted X ray Mössbauer spectrometry
- (c) Emission Mössbauer spectrometry (EMS)
- (d) Conversion (and Auger) electron Mössbauer spectrometry (CEMS)
- (e) Shape of TM or EM spectrum
- (f) Shape of scattering γ ray, X ray or CE Mössbauer spectra

emits the electron from the 1s orbital by an internal conversion process. The energy of the conversion electron is (14.4 - 7.1) = 7.3 keV, where 7.1 keV is the bonding energy of the 1s electron of the ⁵⁷Fe atom. The emission of the conversion electron from the 1s orbital causes transition of the electrons in the 2p, 3p, 4p, ... orbitals to the vacant 1s orbital, resulting in the emission of K_{α} , K_{β} , ... X rays and Auger

CONVERSION ELECTRON

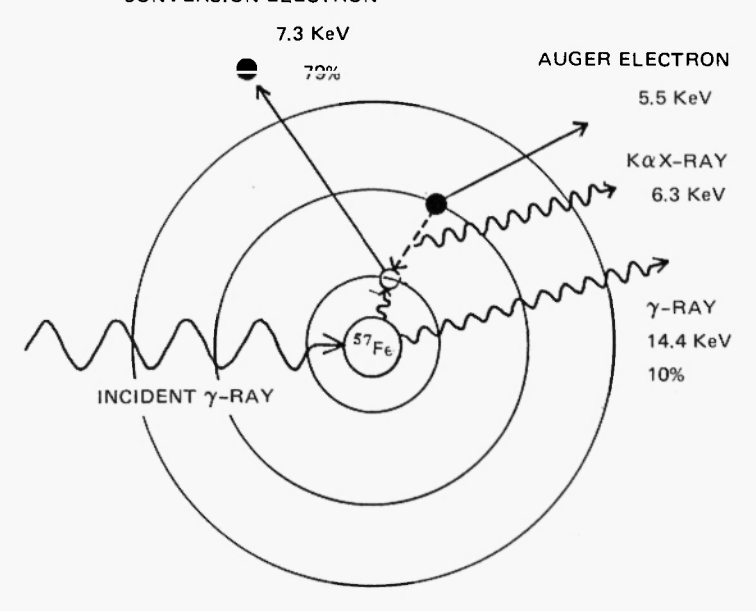


Fig. 2. Deexcitation process of the excited 57 Fe (I = 3/2) nucleus

electrons. The radiations, their intensities and the energies of the reemission processes of excited 57 Fe are listed in Table 1 along with the ranges of the reemitted radiations in metallic iron. Because the γ ray and the conversion electron have different penetration lengths in the solid, scattering Mössbauer spectra of iron can be observed at various depths (10 μ m down to 10 nm) by selecting the detecting radiation $-\gamma$ ray (14.4 keV), X ray (K_{α} ; 6.4 keV) or conversion and Auger electrons (7.3 keV, 5.5 keV).

4. DETECTORS FOR REEMITTED RADIATIONS

4.1. Detection of Reemitted \(\gamma \) Rays

Mössbauer spectra of the ca. 50 μ m depth layer of the solid surface of iron compounds are measured by detecting the reemitted 14.4

TABLE 1

Ranges of radiations re-emitted from the excited ⁵⁷Fe nucleus

nucleus (resonant transition)	radiation	energy (keV)	probability of re-emission	range in metallic iron (nm)
	γ гау	14.4	10%	20000
	K _α X ray	6.3	28%	20000
	K conversion electron	7.3	79%	10 ~ 400
⁵⁷ Fe	L conversion electron	13.5	8%	20 ~ 1300
(14.4 keV)	KLL Auger electron	5.5	63%	7 ~ 200
	LMM Auger electron	0.53	60%	1 ~ 2

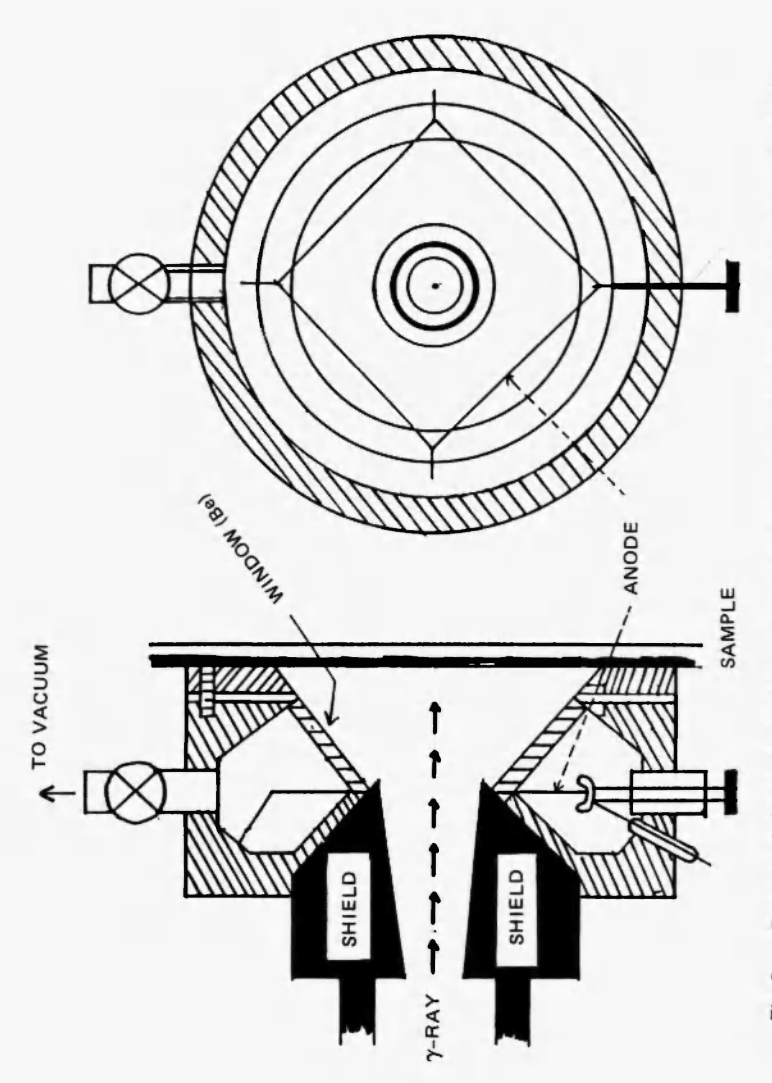
keV γ ray with a 2 inch diameter Kr-filled proportional counter or a 0.5 mm thick NaI (Tl) scintillation counter which is connected to a conventional Mössbauer spectrometer, by adopting the geometrical arrangement shown in Fig. 1-b.

4.2. Detection of Reemitted X Ray

The high radiation yield of the K_{α} X ray reemitted from excited ⁵⁷Fe has encouraged us to measure the Mössbauer spectrum by detecting the X ray. Fujio attempted to establish X ray Mössbauer spectrometry (XMS) and succeeded /15/. An ingenious 99% Kr + 10% CH₄ filled proportional counter for the XMS was designed by Keisch for the non-destructive analysis of the pigment in paintings and iron compounds in terra cotta statuary through the observation of the XM spectra /16, 17/. Sectional views of the details of the XMS detector designed by Keisch are shown in Fig. 3.

The detector was operated at 1000 V by applying 300 V to the guard-grid. The peaks due to the 14.4 keV γ ray and 6.3 keV X ray were resolved distinctly because the FWHM of these peaks were less than 1.8 keV.

Both gas-filled and gas-flow type proportional counters can be used to detect the 6.3 keV K_{α} X ray /18/. The counter, sold by Austin Scientific Associates (BSD 2400), has the anode stretched just outside of the incident γ ray beam and can detect the 14.4 keV γ ray and the 6.3 keV X ray by following PR gas (90% Ar + 10% CH₄).



Detector designed for resonantly scattered γ rays and reemitted X rays (cited from ref. /16/) Fig. 3.

XM spectra of stainless steel, covered with 0.5 μ m and 1.3 μ m of iron foils, shown in Fig. 4 /18/, prove that the effective penetration depth of the X ray in the iron is around 1.5 μ m.

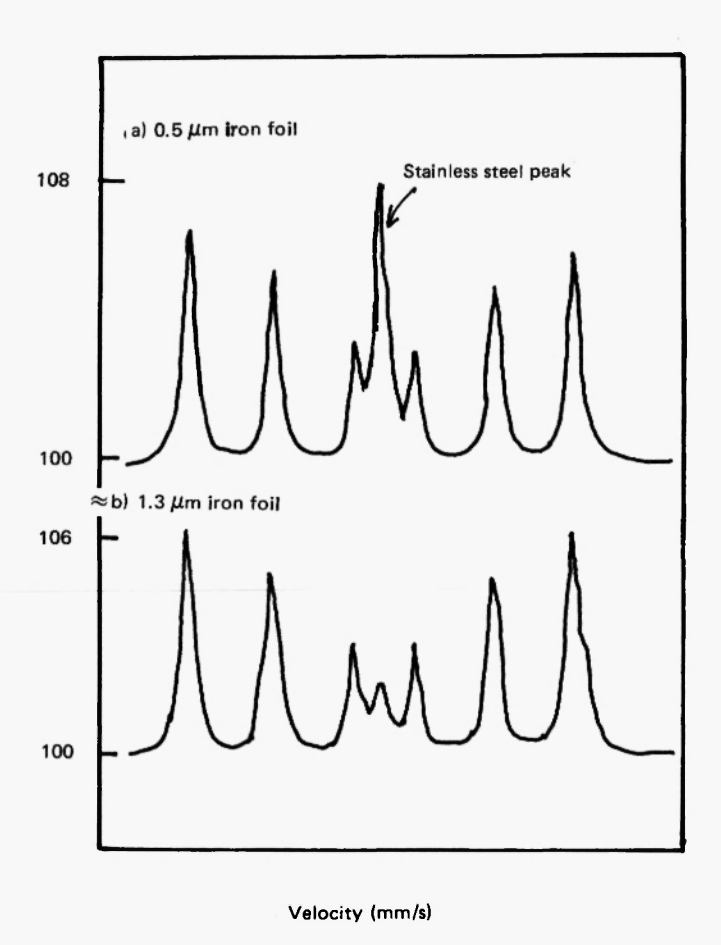


Fig. 4. X ray Mössbauer spectra of stainless steel covered with 0.5 μm and 1.3 μm iron foil (cited from ref. /18/)

4.3. Detectors for Conversion and Auger Electrons

Because the penetration depth of the 0 \sim 7.3 keV electron reemitted from the excited ⁵⁷Fe nucleus is only several tens of nm, electrons are detected by setting the solid sample in the counter or in vacuum. The gas-flow proportional counter, an electron multiplier or a plastic scintillation counter are utilised for the detection of electrons emerging from the solid surface. One of the most useful detectors is the pan-cake shaped gas-flow counter (ϕ 50 mm × 20 mm). The cross-sectional view of a typical counter is shown in Fig. 5 /19/. 90% He-10% CH₄ or Q gas (99% He-1% i-C₄H₁₀) is passed into the counter, since these gases are sensitive enough to detect electrons of several keV but quite insensitive to the detection of co-existent γ - and X-rays.

The tubular electron multiplier made of coated glass tube (delivered from Galileo Electro-Optics Corp., U.S.A. by the name of 'Channeltron') or the ceramics tube (fabricated by Murata Seisakusho, Japan, and called 'Ceratron') has been used in conversion electron Mössbauer spectrometry /20, 21, 22, 23, 24, 27/. A schematic diagram of the chamber used for the detection of reemitted electrons using the Channeltron designed by Massenet is shown in Fig. 6 /25, 26/. The detector is operated in vacuum and allows measurement down to 4.2 K by cooling the specimen in a cryostat /26/. If retarding, reflecting and supressing grids are attached in front of the specimen, the energy spectrum of reemitted electrons from the sample can be measured /26, 27, 28/.

5. DEPTH SELECTIVE OBSERVATION OF SURFACES BY CEMS

Resonantly emitted conversion electrons lose their energy during movement in the solid layer by interaction with the surrounding atoms. The extent of the energy decrease of the conversion electron is dependent on the length of path it has travelled in the solid and it is concluded that the energy of the conversion electrons at the instant they emerge from the solid surface is a measure of the depth, from which they have been emitted.

Therefore, depth-selective CEM spectra can be observed by selection of the energy of the detected electrons. The energy selection is carried out either by applying an electromagnetic /29/ or electro-

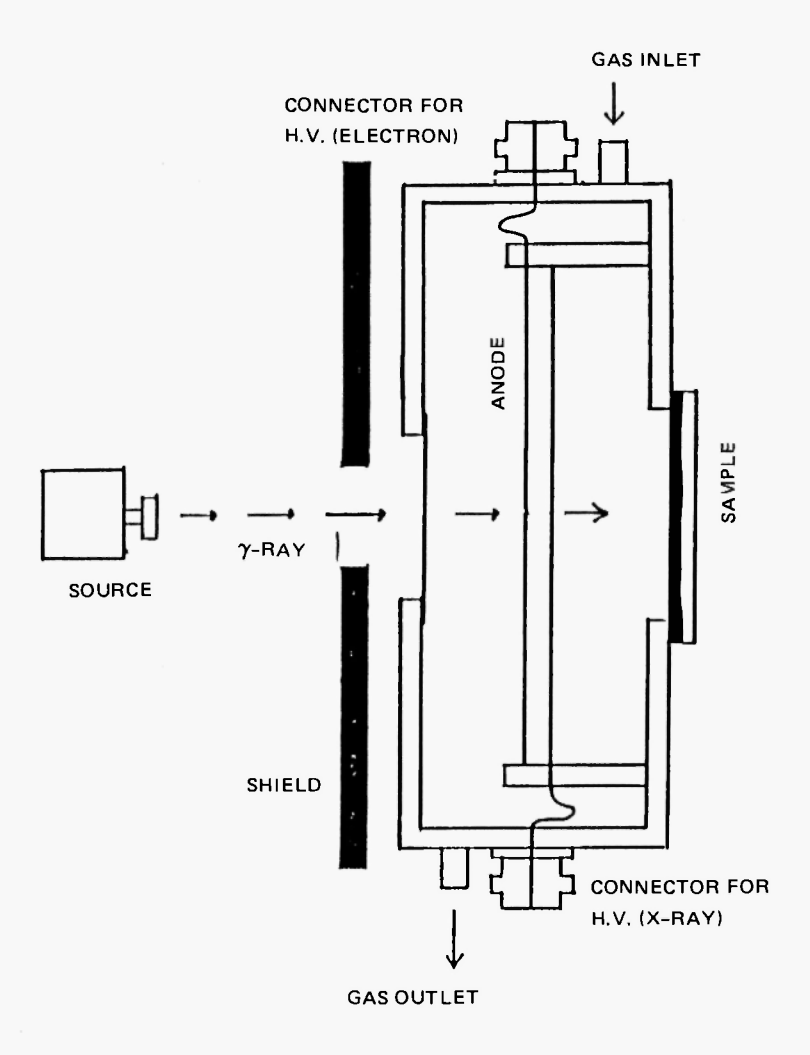


Fig. 5. Backscattering type gas flow proportional counter designed to detect conversion and Auger electrons or X rays.

static /30/ field to the emerging electrons, or by using a pulse height analyser circuit /31/. The electron energy spectra detected by back scattering type gas-flow proportional counters and CEM spectra taken

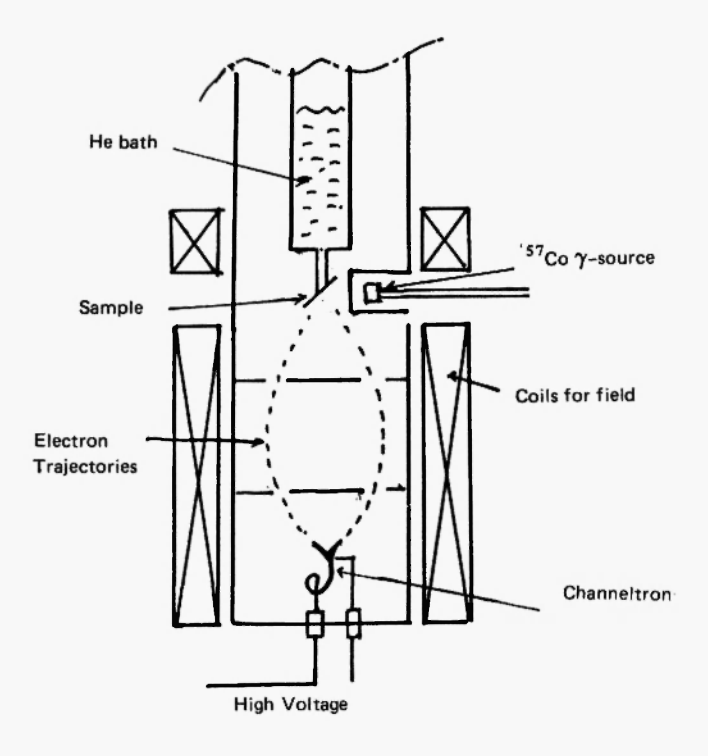


Fig. 6. Apparatus for the measurement of CEM spectra at low temperatures (cited from ref. /26/)

for the specimen prepared by vacuum-deposition of α -Fe (six peaks) on commercial stainless steel foil (single peak) are shown in Fig. 7 /32/. The evidence that the higher the energy of detected electrons, the stronger the peak intensity ratio of α -Fe/stainless steel suggests that depth-selective observation of the surface can be achieved by CEMS.

The penetration depth of the conversion electron was estimated experimentally using stainless steel coated with $20 \sim 100$ nm thick iron /33/. The ratio of the singlet peak of austenite stainless steel to the sextet peaks of α -iron decrease according to the increase of

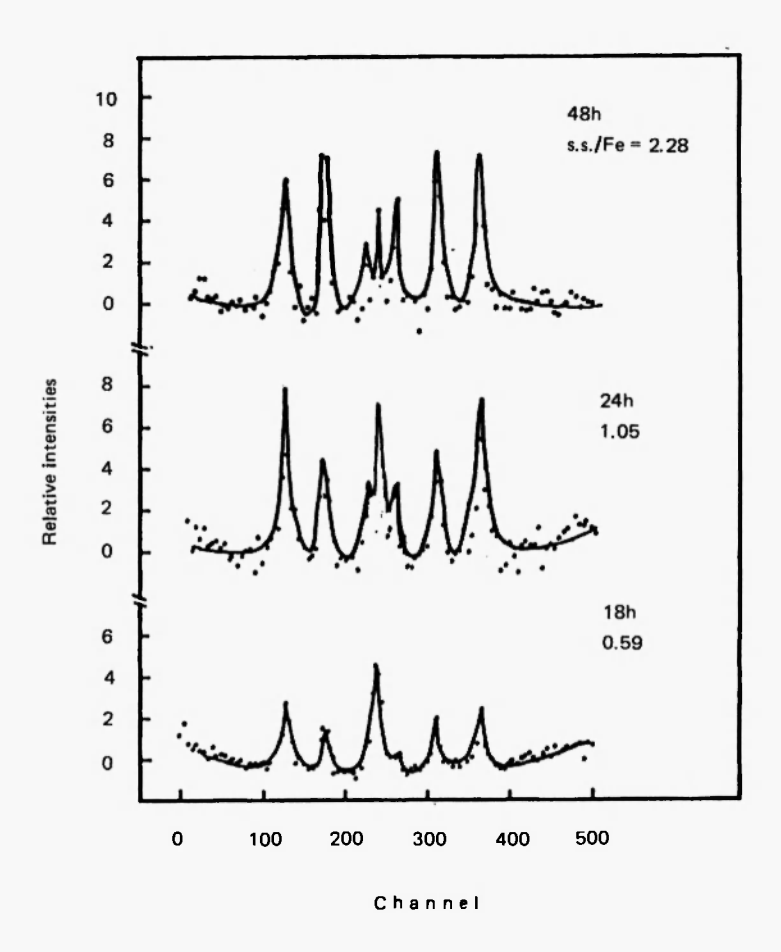


Fig. 7. Energy spectrum of electrons reemitted from the solid sample into the counting chamber, and CEM spectra, observed for stainless steel covered by vacuum-deposited 60 nm α -Fe, by detecting (a) lower, (b) medium and (c) higher energy electrons (cited from ref. /32/)

the thickness of the iron coating. The detection limit thickness of iron is estimated to be 5 nm and 65% of the electron, resonantly reemitted from stainless steel are attenuated by a 43 nm thick iron coating.

The combination of an electron multiplier with a cylindrical mirror electron energy analyser allows us to obtain a very precise depth

selective conversion electron Mössbauer spectrum as illustrated by Kreune's group /34/.

6. MÖSSBAUER PARAMETERS /1, 2, 3, 4, 5/

5.1. Isomer Shift (I.S. or δ)

The 1s electron density at the position of the nucleus varies according to the chemical state of the Mössbauer atom in the sample. The variation of the interaction between the 1s electron and the nucleus causes an energy level shift of both the excited and ground states of the nucleus and results in a variation of the transition energy between the ground and excited levels. Therefore, he resonant absorption peak shifts among compounds if the chemical states differs from one to the other. The isomer shift is represented with respect to reference compounds (α -Fe for 57 Fe, BaSnO₃ for 119 Sn) as follows,

I.S. =
$$\frac{2}{5}\pi Ze^2 (R_{(x}^2 - R_g^2) [\psi_s^2(0) - \psi_s^2(0)]$$
 (1)

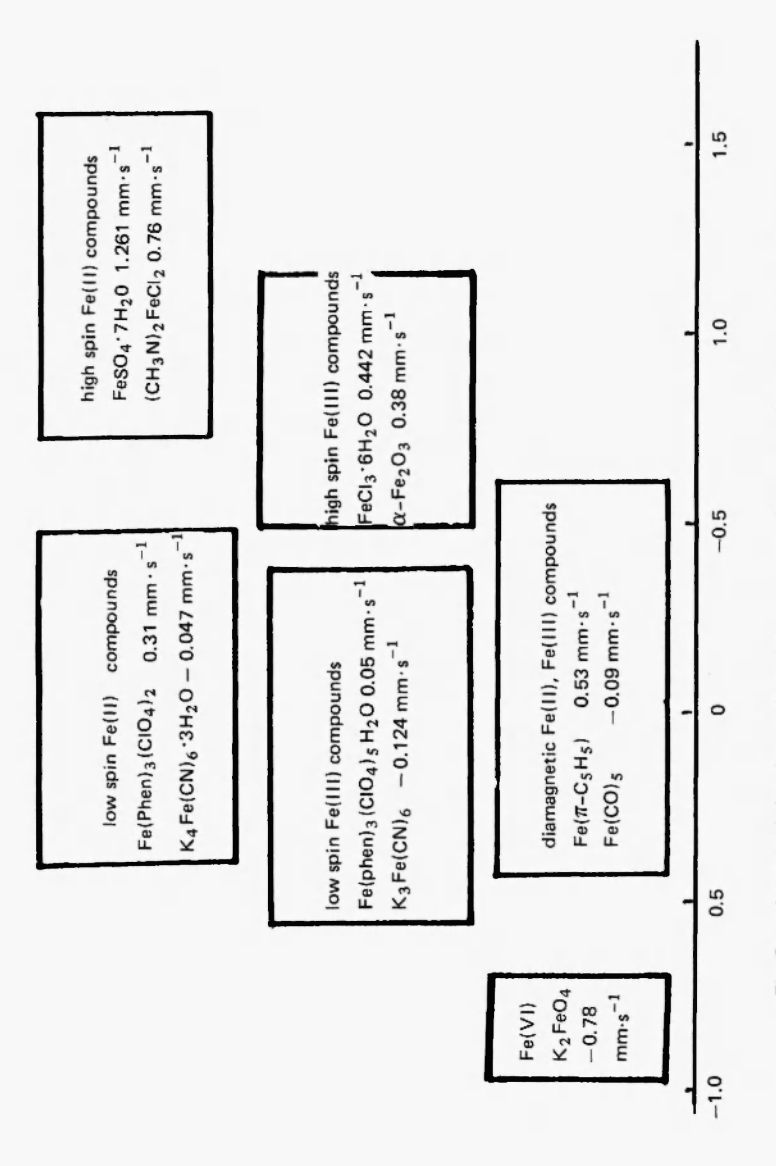
where Z is the atomic number of the Mössbauer atom, e is the charge of the electron (1.6 \times 10⁻¹⁹ C), R_{ex} and R_g are the radii of the Mössbauer nucleus in the excited and ground states respectively, $\psi_s^2(0)$ and $\psi_r^2(0)$ are the s-electron densities at the position of the nucleus of the sample and reference material, respectively. The isomer shifts of typical iron compounds at room temperature are summarized in Fig. 8.

6.2. Magnetic Splitting (Represented in Terms of Internal Magnetic Field, H_{int})

A nucleus with a spin quantum number above 1/2 has a magnetic dipole moment (μ) , which is the origin of nuclear para magnetism. The nuclear magnetic moment is expressed as

$$\mu = g_n I \mu_N$$

where g_n is the nuclear g factor and μ_N is the nuclear magneton $[(eh/2m_p) = 5.05 \times 10^{-27} \text{ J} \cdot \text{T}^{-1}]$. The magnetic dipole moment of the ground and excited state of ⁵⁷Fe, shown in Table 2, interacts



Isomer shifts for various iron campounds measured at room temperature Fig. 8.

TABLE 2

Nuclear magnetic dipole moment (μ) and nuclear electronic quadrupole moment (Q) for typical Mössbauer nuclei

nucleus	nuclear spin (h)	Isotope abundance (%)	variation of radius by excitation $(\frac{R_{ex} - R_g^2}{R_g^2} \times 10^4)$	$\mu^{\mathrm{ex}}_{\mathrm{and}}$ and $\mu^{\mathrm{g}}_{\mathrm{N}}$	Q ^{ex} and Q ^g (barn)
⁵⁷ Fe	(3/2) (1/2)	2.17	-11.6	-0.155 (0.09	(0.21 (0)
¹¹⁹ Sn	(3/2) (1/2)	8.58	3.5	0.68 (-1.05	-0.07 (0)
¹⁸¹ Ta	(^{9/2})	99.99	2.36		3.9

 $\mu_{
m N}$: nuclear magneton (5.051 x 10⁻²⁷ J·T⁻¹)

barn: 10⁻²⁸ m²

with the internal and external magnetic field (H), and results in Zeeman splitting of the nuclear energy levels. The Eigen values of the split nuclear levels are expressed as follows,

$$\mathbf{E}_{\mathbf{m}} = -\mu \cdot \mathbf{H} \cdot \cos \theta = -\mu \cdot \mathbf{H} \cdot \frac{\mathbf{m}}{\mathbf{I}} = -\mathbf{g}_{\mathbf{n}} \cdot \mu_{\mathbf{N}} \cdot \mathbf{H} \cdot \mathbf{m}$$
 (2)

As the nuclear spin quantum number for the ground and first excited levels (14.4 keV) of 57 Fe are 1/2 and 3/2, respectively, these levels split to 2 and 4 levels as depicted in Fig. 9. The 6 transitions can be observed among the 4 split excited levels and 2 split ground levels, because the selection rule, $\Delta m = 0$ or 1, inhibits the transitions between $-1/2 \leftrightarrow 3/2$ and $+1/2 \leftrightarrow -3/2$ level. The energy difference between the 2 split ground levels (ΔE_g) is expressed as

$$\Delta E_g = E_{+\frac{1}{2}}^g - E_{-\frac{1}{2}}^g = (E_{+\frac{1}{2}}^{ex} - E_{-\frac{1}{2}}^g) - (E_{+\frac{1}{2}}^{ex} - E_{+\frac{1}{2}}^g) =$$

$$= -2\mu H \tag{3}$$

and estimated by the energy difference between peaks 2 and 4.

Therefore we can calculate the magnetic field strength by use

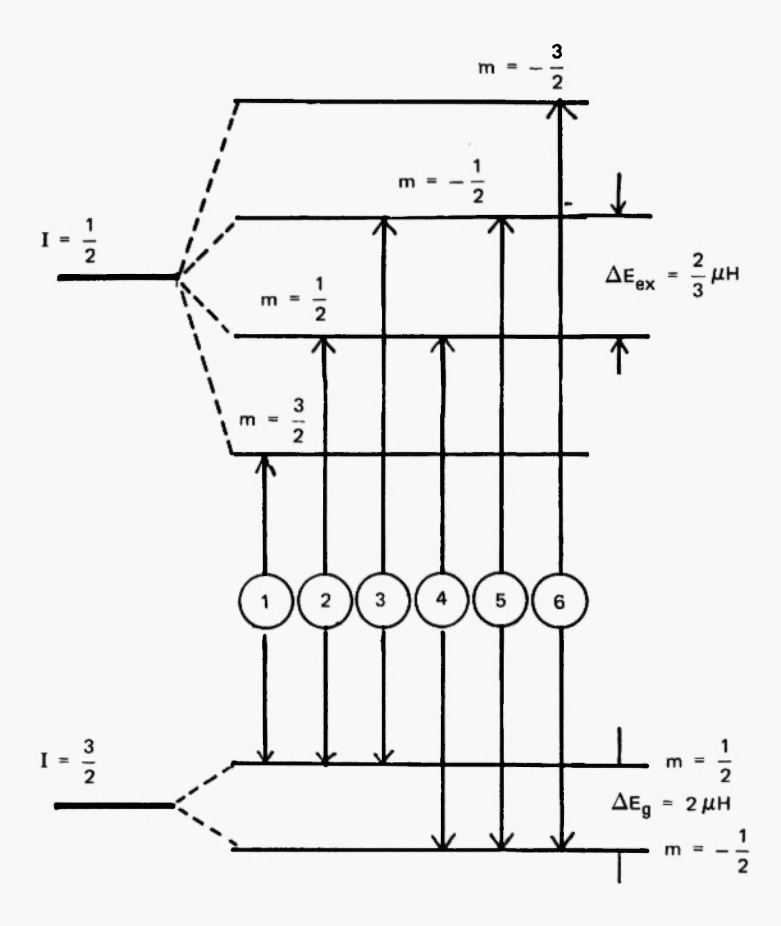


Fig. 9. Splitting of Mössbauer peak, by the magnetic hyperfine interaction for the I = 3/2 \leftrightarrow I = 1/2 transition ($\mu^9 > 0$, $\mu^{ex} < 0$ as for ⁵⁷Fe) _____

of equation (3) and the magnetically split Mössbauer peaks. The relative probabilities of the transitions are summarized in Table 3, and illustrated in Fig. 10. The internal magnetic fields (H_{int}) of certain iron compounds are extremely big even at room temperature as shown in Table 4.

TABLE 3 Rela ive peak intensities for the transition between I = $3/2 \leftrightarrow I = 1/2$

Transition	+3/2 ↔ +1/2	+1/2 ↔ +1/2	$+3/2 \leftrightarrow +1/2 + 11/2 \leftrightarrow +1/2 \leftrightarrow +1/2 \leftrightarrow +1/2$		$+1/2 \leftrightarrow -1/2 \qquad -1/2 \leftrightarrow -1/2 \qquad -3/2 \leftrightarrow -1/2$	-3/2 ↔ -1/2
Peak	1	2	3	4	5	9
Δm	+1	0	+1	+ 1	0	±1
inter sity ratio	$\%(1+\cos^2\theta)$	$\theta_{\rm in}^2 \theta$	$\frac{1}{4}(1+\cos^2\theta)$	$1 + \cos^2 \theta$	$\theta_{z}^{u_{i}}$	$\%(1+\cos^2\theta)$
random *	ю	: 2	. 1	1	: 2	3
$\theta = 0$	ю	0 :	: 1	1	0 :	
$\theta = 60$	3	4		-	4	

* For a random y picked polycrystalline sample, $\langle \cos^2 \theta \rangle = 1/3$ and $\langle \sin^2 \theta \rangle = 2/3$

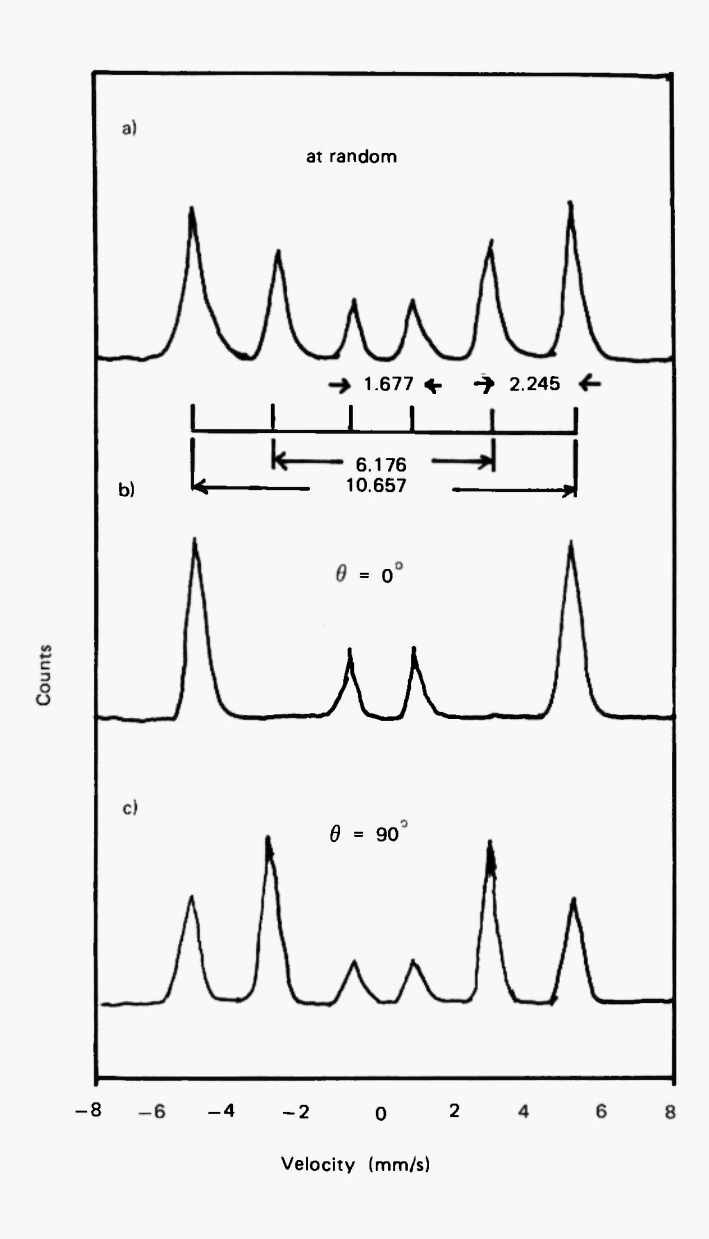


Fig. 10. Variation of relative intensities among magnetically split peaks as a function of the angle between the incident γ ray and the principal axis of the magnetic field

TABLE 4

Mössbauer parameters of typical iron oxides and oxyhydroxides
at room temperature

compounds	I.S. $(\alpha$ -Fe) $(mm \cdot s^{-1})$	$Q \cdot S$ (mm · s ⁻¹)	H _{int} (T)	Neel temp.* (K)
α-Fe ₂ O ₃	0.42	0.12	51.8	956
	0.27	_	48.8	0.56
γ -Fe ₂ O ₃	0.41		49.9	856
			49.1	453
Fe ₃ O ₄ **			45.3	491
α-FeOOH	0.61		38.9	393.3
β-FeOOH	0.39	0.62	0	270
γ-FeOOH	0.38	0.60	0	50
δ-FeOOH				
Fe(OH) ₂	1.18	2.92	200	34
Fe(OH) ₃	0.33	0.66	_	

^{*} Magnetic transformation for anti-ferromagnetic substance

6.3. Quadrupole Splitting (Q.S. or Δ)

A nucleus with a spin quantum number greater than 1 is not necessarily spherical and has a nuclear quadrupole moment (Q) expressed as

$$Q = \int_{\tau} [(z^2 - x^2) + (z^2 - y^2)] d\tau = \int_{\tau} (3z^2 - r^2) d\tau$$
 (4)

The Q's for the ground and excited ⁵⁷Fe nucleus are shown in Table 3.

Q interacts with the electric field gradient expressed as efg or q, originating from the asymmetric distribution of electrons around the nucleus, to result in splitting of the energy level of nuclei with I > 1. The energy shift of the split levels is expressed as

$$E_{Q} = \frac{e^{2}qQ}{4I(2I-1)} \left[3m^{2} - I(I+1)\right] \left(1 + \frac{\eta^{2}}{3}\right)^{\frac{1}{2}}$$
 (5)

where, I is the nuclear spin quantum number, m the quantum state with a value I, I - 1, - (I - 1), -I and η is the asymmetric factor defined by $(q_{xx} - q_{xy})/q_{zz}$.

^{**} Ferrimagnetism

For ⁵⁷Fe, the energies for the quadrupole split levels of the excited I = 3/2 (m = $\pm 3/2$ and $\pm 1/2$) state and the ground I = 1/2 (m = $\pm 1/2$) state are calculated as,

$$E_{\pm 3/2}^{\text{ex}} = + \frac{e^2 Qq}{4} \left(1 + \frac{\eta^2}{3}\right)^{1/2}$$
 (6)

$$E_{\pm \frac{1}{2}}^{\text{ex}} = -\frac{e^2 Qq}{4} \left(1 + \frac{\eta^2}{3}\right)^{\frac{1}{2}}$$
 (7)

therefore, the transition energy difference between the quadrupole split $(\pm 3/2)$ and $(\pm 1/2)$ levels is expressed as

$$\Delta E_Q = E_{\pm 3/2}^{\text{ex}} - E_{\pm \frac{1}{2}}^{\text{ex}} = \frac{e^2 qQ}{2} \left(1 + \frac{\eta^2}{3}\right)^{\frac{1}{2}}$$
 (8)

A schematic diagram of the energy level splitting by the nuclear quadrupole interaction and the allowed transitions is illustrated in Fig. 11. The value of q is large for high spin Fe(II) compounds, very small for Fe(III) compounds and almost zero for diamagnetic Fe(CN) $_{5}^{3}$, Fe(CN) $_{5}^{4}$, or organic iron compounds as listed in Table 2. The peak intensity ratio of the quadrupole split peak depends on the angle

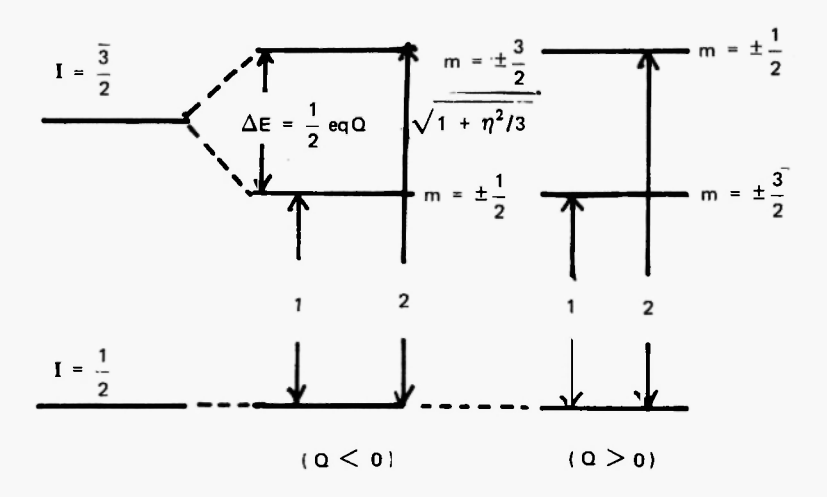


Fig. 11. Quadrupole splitting for the I = 3/2 \leftrightarrow I = 1/2 transition caused by the interaction between the nuclear quadrupole moment (Q) and the electric field gradient (q = $\partial E/\partial Z = \partial^2 V/\partial Z^2$)

(θ) between the directions of the incident γ -ray and the quantum axis of the efg of the sample (Table 5).

TABLE 5
Relative intersities for quadrupole split peaks of (I = $3/2 \leftrightarrow I = 1/2$) transition

Transition	$(m = \pm 3/2) \leftrightarrow (m = \pm 1/2)$		$(m = \pm 1/2) \Leftrightarrow (m = \pm 1/2)$
Transition probability for $\eta = 0$	$\frac{3}{2} \left(1 + \cos^2 \theta \right)$:	$1 + \frac{3}{2} \sin^2 \theta$
random	1	:	1
$\theta = 0$	3	:	1
$\theta = 90$	3	:	5

7. APPLICATIONS

7.1. Orientation of the Magnetic Field (Axis of Quantization) of Iron and Steel at the Surface

X-ray and conversion electron Mössbauer spectra of α -iron and steel have magnetically split sextet peaks as shown in Fig. 12 /35/. The difference in the relative intensities among the sextet peaks for the TM, XM and CEM spectra originate from the orientational difference of the magnetic axis of ferromagnetic iron grains between the surface and under-layers. Table 3, shows that the transition probability depends on the angle (θ) between the applied internal magnetic field and the incident γ -ray. Because the relative peak intensities of the XM spectrum of polycrystalline iron foil are 3:2:1:1:2:3, similar to those obtained for the TM spectrum, it is suggested that the direction of the magnetic field of iron located in the surface layer of the range of the X-ray ($\sim 20 \mu m$) is random. On the other hand, relative peak intensities of 3:4:1:1:4:3 observed in the CEM spectrum suggest that the internal magnetic field of polycrystalline α -iron, situated less than 100 nm below the surface, orientate parallel to the surface.

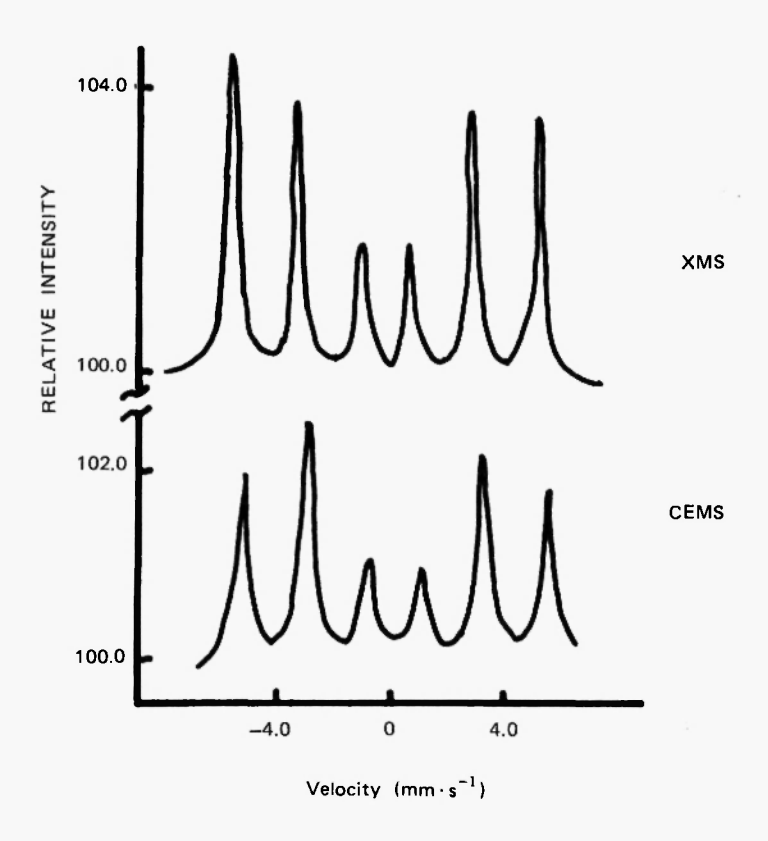


Fig. 12. Relative intensity variation of polycrystalline α-iron for the top 100 nm surface (CEM spectrum) and for the 10 μrn depth layer (XM spectrum) (cited from ref. /35/)

7.2. Characterization of Surface Products on Oxidized Steels

The CEM spectra of plain low carbon steel, heat-treated in air in a muffle furnace at 450°C for 10, 20 or 30 minutes, are shown in Fig. 13. Analysis of the spectra reveals that the steel surface is oxidized by aerial oxygen at high temperature to form magnetite (Fe₃O₄) and hematite (α -Fe₂O₃), and longer oxidation brings about an increase of the thickness of the oxidation layer and the proportion of α -Fe₂O₃ /33/.

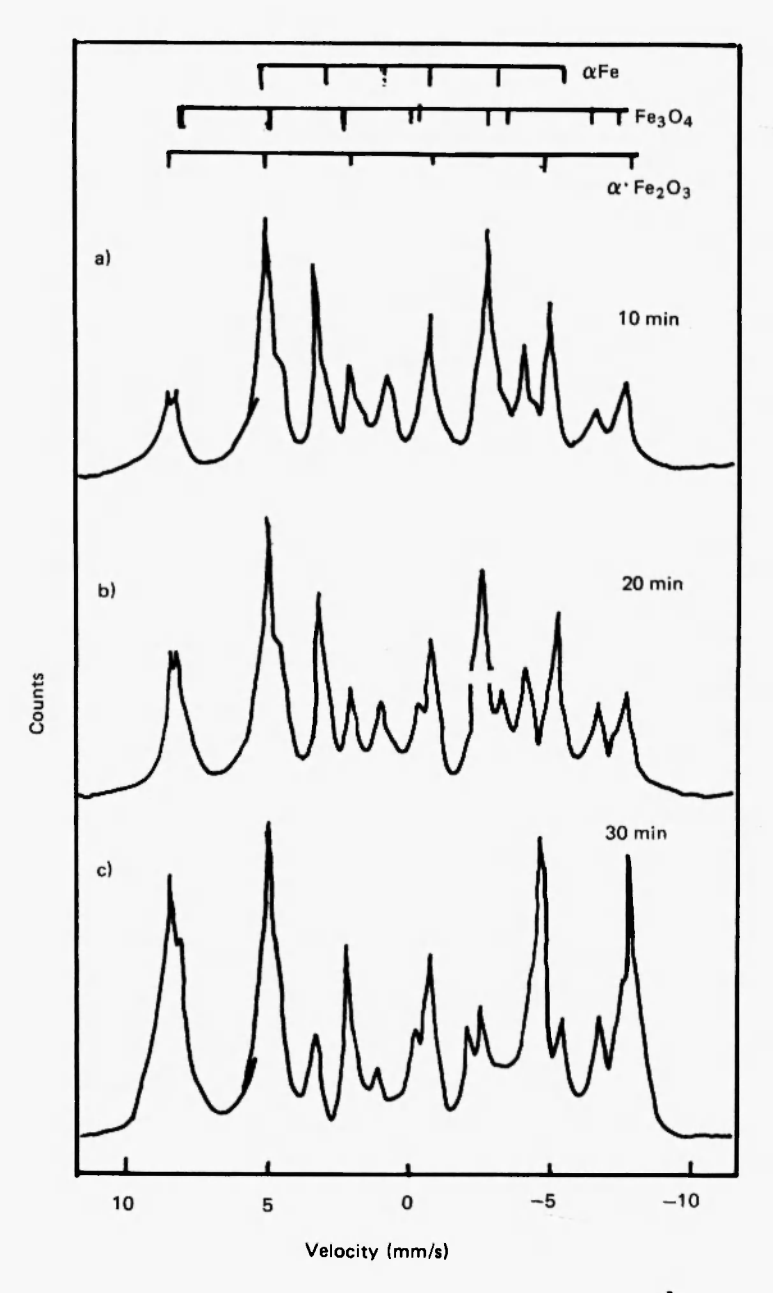


Fig. 13. CEM spectra for an oxidized steel surface heat-treated at 450°C (cited from ref. /33/)

The growth of the protective oxide layers, formed on Fe-Cr (martensite) and Fe-Cr-Ni (austenite) alloys by the action of oxygen-free water at 295° C (1.42×10^{7} Pa, pH 9-10) during a period of 70 hours, was studied by Gutlich *et al.* /36/. The oxide on the surface was identified as Fe_{3-x}O₄ (A site; Fe³⁺, B site; Fe²⁺, Fe³⁺) by analysis of the CEM spectra (Fig. 14).

The analysis of corrosion products, deposited on steel surfaces during immersion in aqueous solutions of various salts, was carried out by Ujihira and Nomura /37/. When polished steel was immersed in deionized water and kept for several tens of hours, γ -FeOOH was observed to form on the surface. The Fe(II) species produced are assumed to be dissolved in the solution, oxidized by dissolved oxygen to Fe(III) ion and then precipitated in the weak acid solution to form γ -FeOOH. The doublet peaks of γ -FeOOH grow with the lapse of immersion time. Similar doublet peaks were observed when the steel was immersed in 0.5M NaCl solution at pH 5.5. The doublet peaks are attributed to γ -FeOOH by the Mössbauer parameter and confirmed by X-ray diffraction patterns of the detached oxidized iron layer. The peaks grow higher with increase of immersion time. β -FeOOH, which is usually produced on the steel surface when corroded in sea water was not found in the corrosion products.

When the steel was dipped in 0.5M NaSO₄ solution, oxidation proceeded slowly and quadrupole split peaks due to Fe(OH)2 were seen in the CEM spectrum (Fig. 15). The gradual decrease of the peak intensity of Fe(OH), and the growth of peaks due to y-FeOOH with immersion time were clearly seen in the CEM spectra. The Fe(OH)₂ once formed was oxidized and converted to γ -FeOOH, When the steel was immersed in 0.5M NaNO₃ solution, oxidation was initiated inhomogeniously on the surface and brown coloured spots of γ -FeOOH spread to cover the whole surface of the steel. Peaks due to magnetite (Fe₃O₄) were seen to develop besides the doublet of γ-FeOOH during 9 hours immersion. The Fe₃O₄ layer, formed in between the γ -FeOOH layer and the steel substrate, grows thicker with increase of immersion time as shown in Fig. 16. When the steel was immersed in 0.5 M NH₄NO₃ solution, the peaks due to paramagnetic iron(III) compounds grow rapidly and the oxidized layer was easily scraped off the substrate. After the peaks of the γ-FeOOH layer had grown, the peaks due to the magnetite layer developed very slowly. The dense and tight γ -FeOOH layer, produced

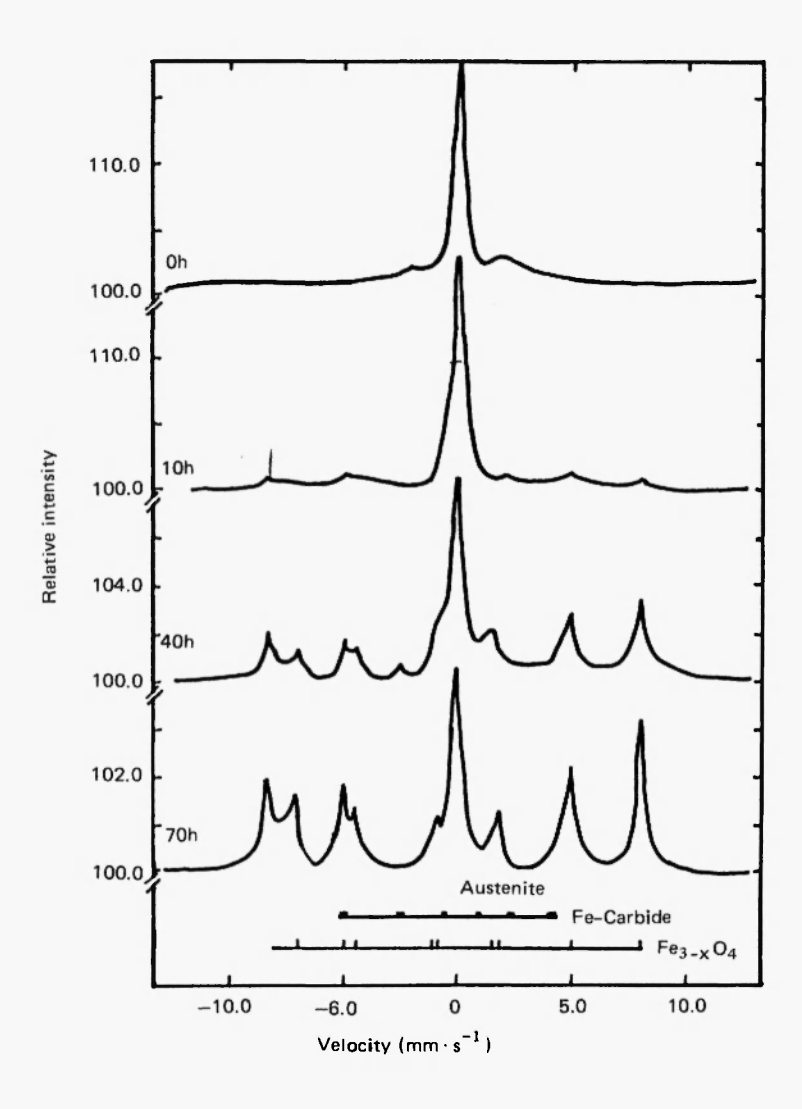


Fig. 14. CEM spectra of stainless steel oxidized in water at 295°C 1.4 x 10⁵ Pa (cited from ref. /36/)

in the first stage of oxidation, is considered to retard the diffusion of dissolved oxygen into the inner layer, and the Fe₃O₄ layer formed

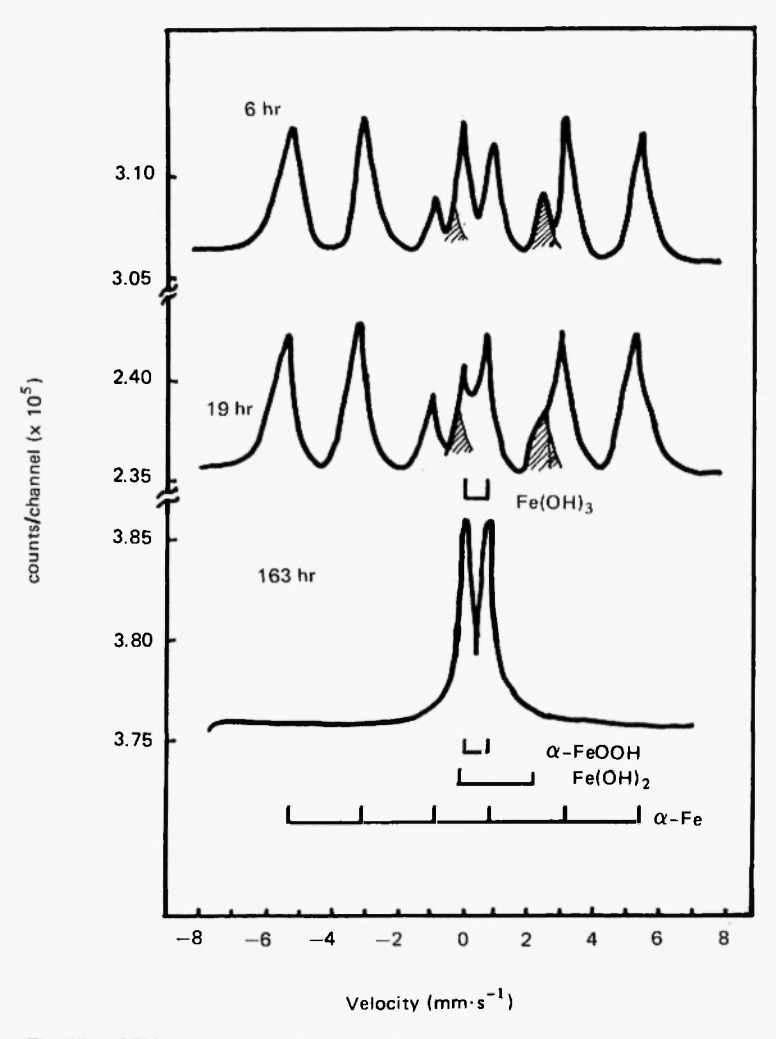


Fig. 15. CEM spectra of steel corroded in 0.5 M Na₂SO₄ solution at room temperature (cited from ref. /37/)

between the γ -FeOOH layer and steel substrate. Specimens were prepared by freeze-drying the oxidized steel in vacuum to avoid further oxidation and shaving off the γ -FeOOH and Fe₃O₄. This procedure allowed the authors to observe the doublet peaks due to the iron(II) compound, which is considered to be produced beneath the Fe₃O₄ layer, in the CEM spectrum.

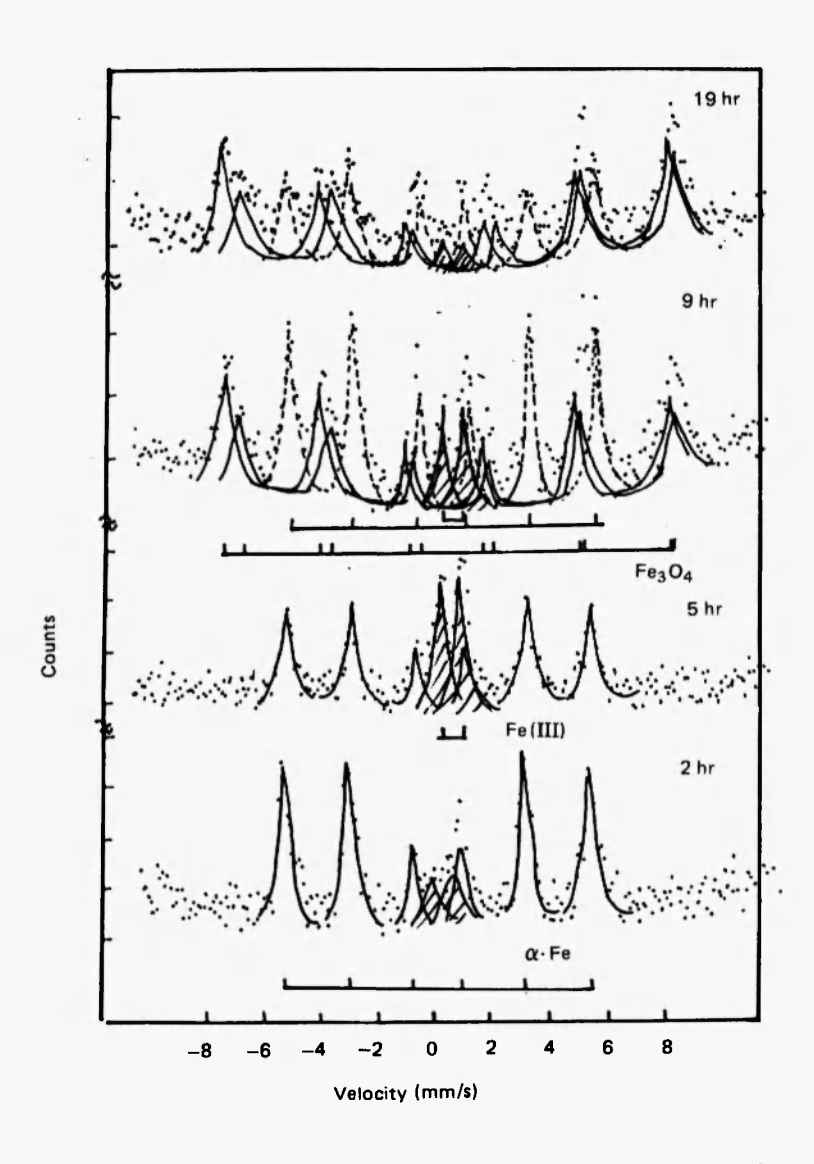


Fig. 16. CEM spectra of steel corroded in 1.0 M NaNO₃ solution at room temperature (cited from ref. /37/)

7.3. Corrosion Study of Steels in Atmospheres Containing HCl, SO_2 or H_2S

The CEM spectra of stainless steel 304 exposed to a moist atmosphere of 5.5×10^3 Pa. HCl for 8 minutes at room temperature followed by standing in air for a day are shown in Fig. 17A /28/. The doublet peaks (I.S.: 1.21 mm·s⁻¹, Q.S.: 2.53 mm·s⁻¹), characteristic of a high spin Fe(II) compound attributable to FeCl₂·2H₂O and doublet peaks with small quadrupole splitting suggesting the presence of β -and/or γ -FeOOH, are seen in the spectrum. The inner doublet peaks of a Fe(III) compound grows following the one day extention of exposure to air as shown in Fig. 17B. The exposure of SM-50 steel to a moist atmosphere containing 5.5×10^3 Pa. HCl for 8 minutes gave large quadrupole split peaks in the CEM spectra and after standing in dry for 10 days two doublet peaks appear in the CEM spec-

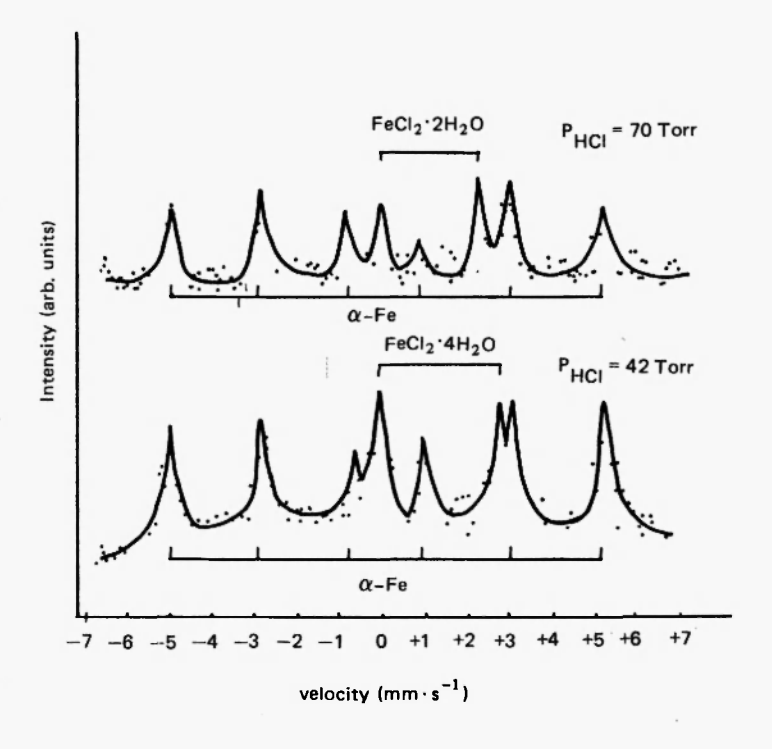


Fig. 17. CEM spectra of a steel surface immediately after exposure to an HCI atmosphere (cited from ref. /28/)

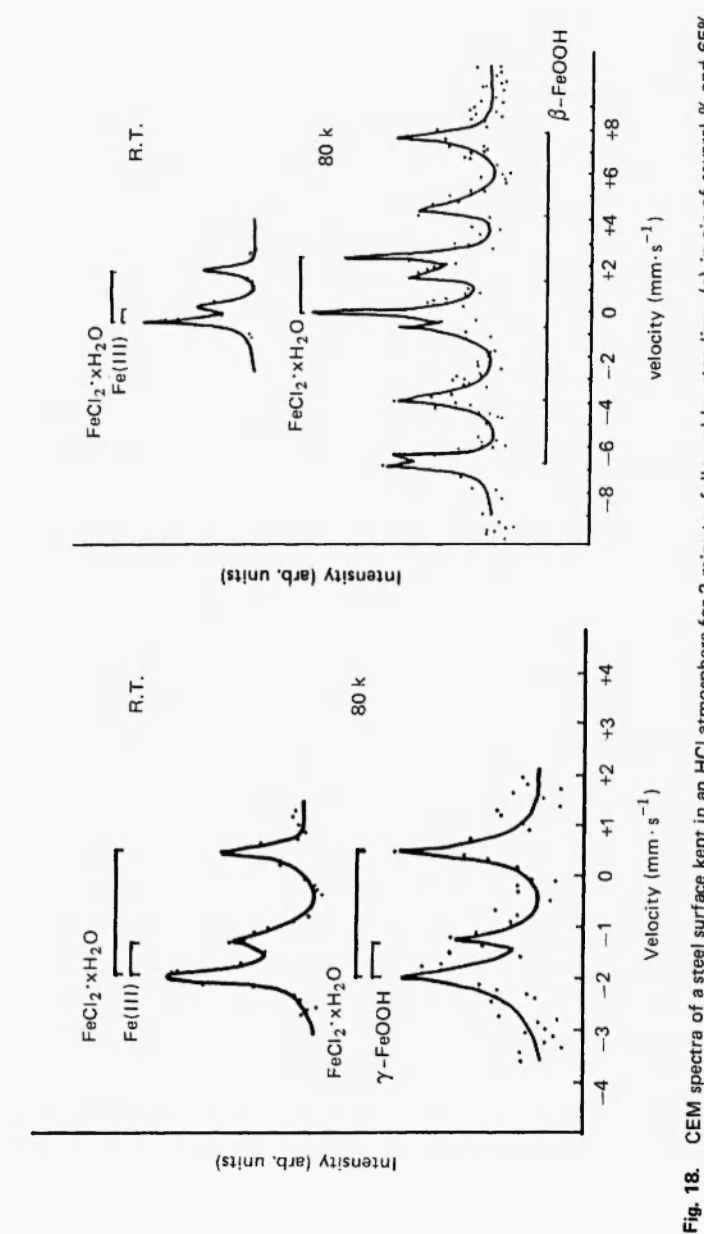
trum. The inner doublet is attributed to FeCl₂ · 2H₂O and the outer doublet to FeCl₂ · 4H₂O. Further exposure of the sample to moist atmosphere diminished the doublet peaks due to FeCl₂ · 2H₂O. After 5 days of exposure, peaks attributable to β - and/or γ -FeOOH appeared in the spectrum. The use of a CEM spectrometer equipped with an electron multiplier as a detector afforded 77 K measurement of the CEM spectrum, which distinguishes β -FeOOH (T_N = 273K) and γ -FeOOH (T_N = 50K) because the former is anti-ferromagnetic and the latter is paramagnetic at 80K. Fig. 18 reveals that the FeCl₂ · 2H₂O film deposited on steel does not change in dry air, but is oxidized to \(\beta\)-FeOOH in an atmosphere of several percent humidity and that the formation of γ -FeOOH begins when the moisture in the atmosphere exceeds several percent and that only γ -FeOOH is produced in air saturated with humidity /28/. Ramshesh et al. by means of TMS and CEMS identified a mixture of β- and γ-FeOOH and perhaps a little α-FeOOH in a corrosion product of mild steel or iron suspended for several hours in 0.1 - 3.5 HCl solution /38/. They also reported the formation of FeCl₂·4H₂O on the surface when the steel or iron was exposed to $3.5 - 8.0 \,\mathrm{M}$ HCl.

The author exposed cold rolled carbon steel sheet to an atmosphere polluted by SO_2 and identified $FeSO_4 \cdot H_2O$ and $FeSO_4 \cdot 4H_2O$ deposits on the steel surface as the initial corrosion product which subsequently transformed to $Fe_4SO_4(OH)_{10}$ /39/. Then, the intermediate iron compound changes to γ -FeOOH to form the final corrosion product (19a). The depth-selective CEM spectrum (Fig. 19b) for the sample corroded in a moist air containing 0.16% of SO_2 for 15 minutes followed by exposure to moist air for 90 minutes revealed that Fe(III) compounds were located at the top surface and that they were substituted by $FeSO_4 \cdot 4H_2O$ and $FeSO_4 \cdot H_2O$ below the surface.

Treatment of the same steel in a gas mixture of H_2S (0.86 vol%) $-N_2$ (99.14 vol%) at 25°C for various periods gave paramagnetic FeS_{1-x} (mackinawite) (\sim 10 nm) at first. It transformed to ferromagnetic mackinawite and then to Fe_3S_4 (greigite) by further corrosion as shown in the CEM spectra (Fig. 20)/40/.

7.4. Analyses of Phosphate and Oxalate Coatings of Steels

The phosphate coating on steel is corrosion-resistant and serves as an appropriate ground material for painting. Iron at the steel surface reacts with cation and phosphate ion in a bath of phosphating solution



CEM spectra of a steel surface kept in an HCl atmosphere for 3 minutes followed by standing (a) in air of several % and 65% humidity for 10 and 7 days, respectively, and (b) in air saturated with water vapor for 15 minutes (cited from ref. /28/)

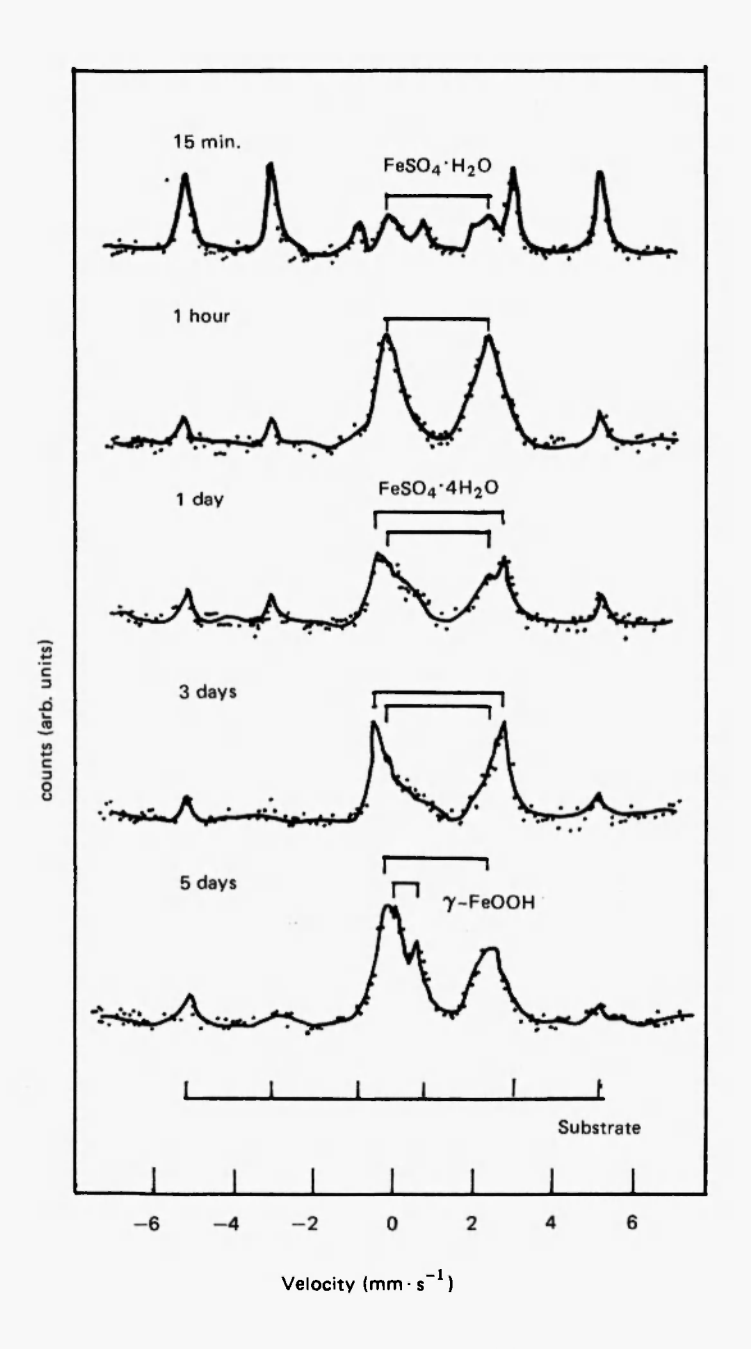


Fig. 19. CEM spectra of a steel surface corroded (a) in moist air containing 1600 ppm SO₂ during various periods at room temperature and (b) the depth selective CEM spectra of 19- sample (cited from ref. /39/)

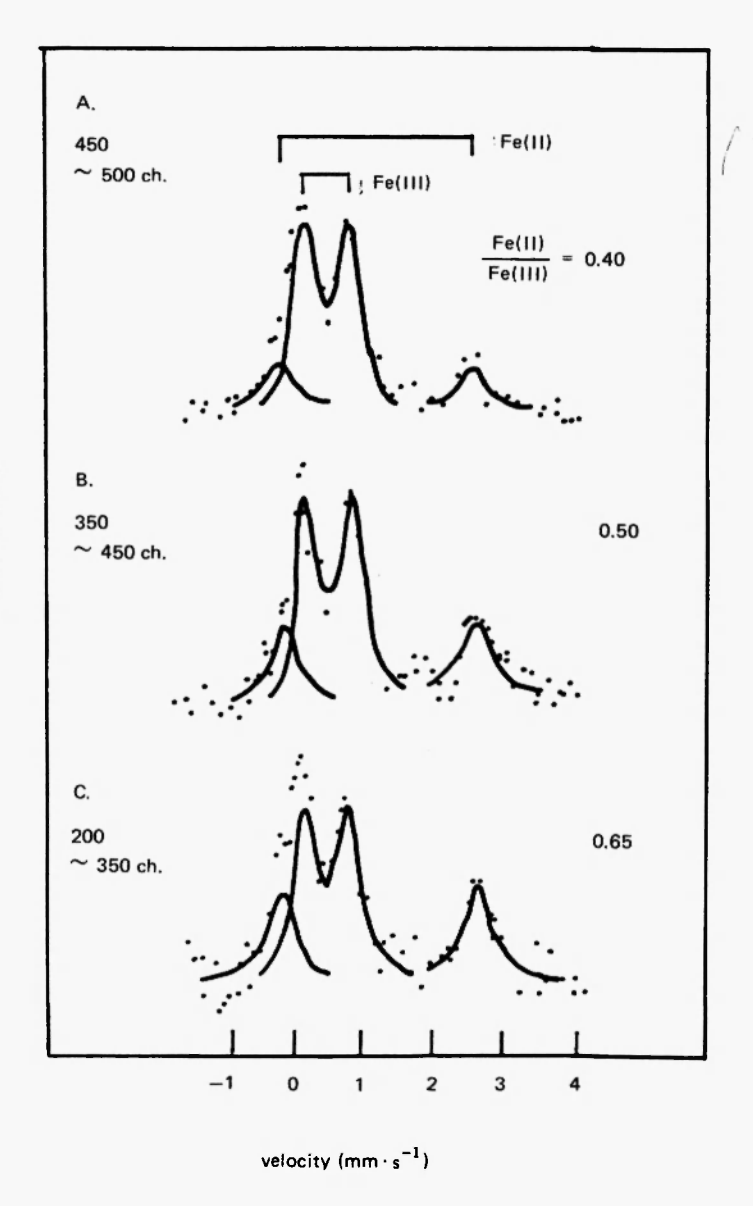


Fig. 19. cont.

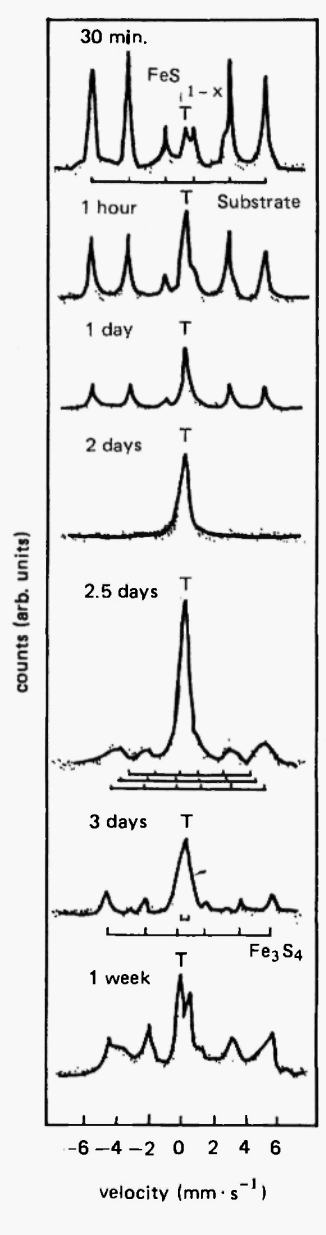


Fig. 20. Variation of CEM spectra of steel surface corroded in H_2S (0.86 vol%)- N_2 (99.14 vol%) environment for various periods at room temperature (cited from ref. /40/)

and cation-iron-phosphate compounds are deposited as a coating at the steel surface. CEMS has been applied to the chemical state analysis of iron in the phosphate coatings, which are produced on surfaces of rimmed or cold rolled steels by immersion in phosphoric acid, iron phosphate, manganese phosphate or zinc phosphate.

Quadrupole split peaks of Fe₃(PO₄)₂·8H₂O have been observed in the CEM spectrum of iron treated in dilute phosphoric acid /41/.

The immersion of steel in an iron phosphate bath produced an amorphous Fe(III) compound which gave doublet peaks characteristic of a paramagnetic Fe(III) compound /42/.

Three sets of quadrupole split peaks appeared in the CEM spectrum of steel dipped in a manganese phosphating bath and they were assigned to the Fe(II) of a high spin Fe(II) compound occupying three different sites in the crystal lattice of hureaulite $[(Mn,Fe)_5H_2(PO_4)_4\cdot 4H_2O]/43,44$.

The following reaction was presumed to proceed when the steel was immersed in a zinc phosphating bath.

2Fe +
$$3Zn^{2+}$$
 + $4H_2PO_4$ + $2NO_3$ →
→ 2FePO₄ + $Zn_3(PO_4)_2$ + $2NO$ + $4H_2O$
(sludge) (coating)

As the initial step of zinc phosphating, the dissolved Fe(III) ions, liberated from the steel surface are incorporated in the reaction to form monoclinic phosphophyllite, $Zn_2Fe(PO_4)\cdot 4H_2O$, which grows epitaxially, and then the main product, orthorhombic hopeite, $Zn_3(PO_4)_2\cdot 4H_2O$, is deposited. The CEM spectrum of the zinc phosphated steel reveals the presence of an amorphous Fe(III) compound in addition to phosphophyllite /45/. The growth of a paramagnetic Fe(III) compound and the phosphophyllite in the coating during immersion are shown in Fig. 21 /46, 47/, by Nomura and Ujihira.

The thermal deterioration of zinc phosphate coating has been studied in detail /48/.

The oxalate treatment is widely applied to stainless steel to produce a coating, that reduces the friction generated by plastic deformation and serves as a surface lubricant. The CEM spectrum of oxalated steel shows quadrupole split peaks of $FeC_2O_4 \cdot 2H_2O$. The chemical state of Fe(II) in the oxalate coating is not affected by the rolling process /49/.

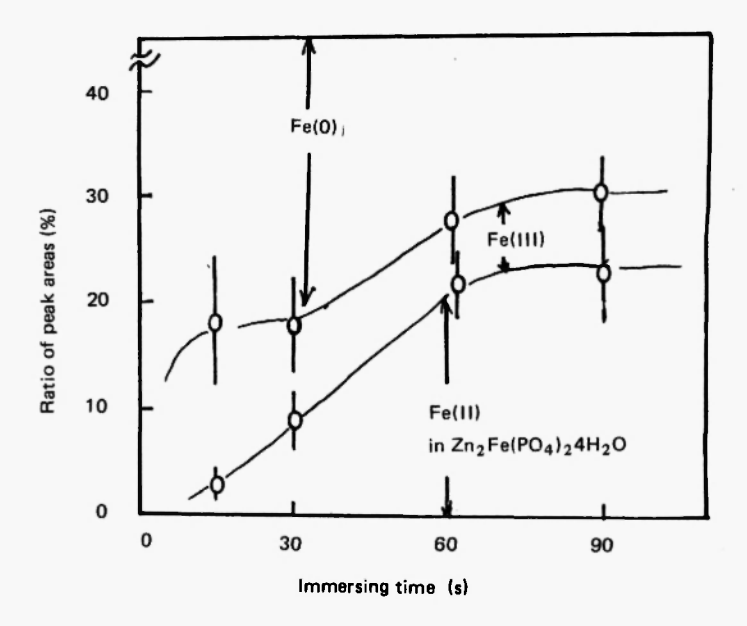


Fig. 21. Relation between the duration of phosphating and the percentage of three Fe states in zinc phosphate coating (cited from ref. /45/)

7.5. Analysis of Hardened Steel Surfaces

The surface of gear wheels, crankshafts, etc. are hardened by the introduction of boron, carbon or nitrogen to the crystal structure of the steel to form compound layers between 10 μ m to 1 mm thick at the surface. CEM analysis of the iron compounds deposited on the surface through the solid phase reaction of steel (SCM3) and B₄C powder at 900°C for 5 hours /50/ (after grinding the surface to various depths) is shown in Fig. 22. Because an increase of the boron content decreases the strength of the internal magnetic field in the iron-boron system, the uppermost layer with the smaller internal magnetic field, Fig. 22, is attributed to FeB_x (x > 1). The CEM spectrum of the exposed layer after grinding 5 μ m off the top surface shows the magnitude of the internal magnetic field corresponding to FeB. The CEM spectra of the 20 μ m, 33 μ m, 89 μ m and 130 μ m deep layers suggest the presence of superposition of both



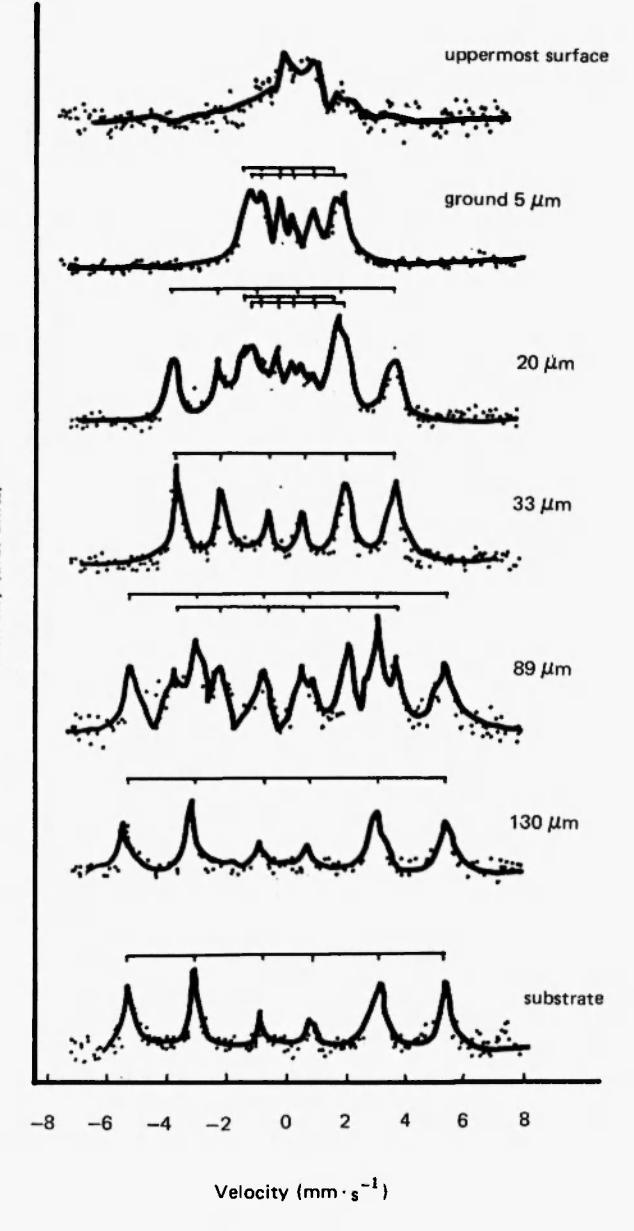


Fig. 22. CEM spectra of a borided steel surface observed after the removal of desired thickness by grinding with SiC powder (cited from ref. /50/)

FeB and Fe₂B at 20 μ m depth, the existence of only Fe₂B at 33 μ m depth, and the formation of a Fe₂B and α -iron layer with the Fe₂B/ α -Fe ratio decreasing towards zero at 80 \sim 130 μ m depth.

Similar multi-layer structures were observed for borided Armco iron (prepared by heating at 1000° C in vacuum with boron powder for 15 hours) by applying CEMS, XMS, and TMS to the detached 10 μ m film layer /50/. Three distinct compound layers – FeB_x (~ 30 μ m), FeB (~ 5 μ m), Fe₂B (~ 15 μ m) – were identified /51/.

CEMS has been applied to the analysis of the physico-chemical state of a steel surface after carburization by heating H-2 steel at 930°C for 2 hours in a mixture of propane and air using nickel as a catalyst, followed by quenching in oil and reheating at 880°C for 15 minutes to remove strain in the steel /52/. The X-ray diffraction pattern, observed for the carburized steel, indicated the composite existence of γ -austenite and α '-martensite at the surface but the diffraction peaks of α '-martensite could not be distinguished from that of α -iron. The CEM spectrum of the uppermost surface, however, reveals that the singlet peak of γ -austenite is prevalent and the sextet peak of α '-martensite, as indicated by the arrows in Fig. 23, is only slightly recognised.

The intensity in variation of superimposed peaks of α '-martensite and γ -austenite for a carburized steel surface as a function of depth, Fig. 23, led us to conclude that the top surface has the higher γ -austenite/ α '-martensite ratio and that the decrease of γ -austenite content is very steep in the range between the top and the 10 μ m deep layers. The result suggests that the top surface cooled down faster during the quenching process than the speed of transformation of γ -austenite to α '-martensite (within 10^{-7} s) resulting in the conservation of paramagnetic γ -austenite at the top surface.

No evidence of the formation of iron carbide or cemetite, ζ -Fe₃C, was recognized.

A multi-layer structure of the hardened surface of nitrided steel was also observed by CEMS /53, 54/. The variation of CEM spectra for gas nitrided steels, prepared by exposing the sample to atomic nitrogen, produced by thermal decomposition of ammonia $(2NH_3 \rightarrow 2N + 3H_2)$ at 520° C for 30 hours, is shown in Fig. 24(a). The surface layers were ground off to the desired thickness with SiC 500 powder. Analysis of Fig. 24(a) shows evidence of the existence of 4 distinct layers. The compound produced at the top surface is identified as paramagnetic ϵ -Fe₂N, the thickness of which was estimated to be

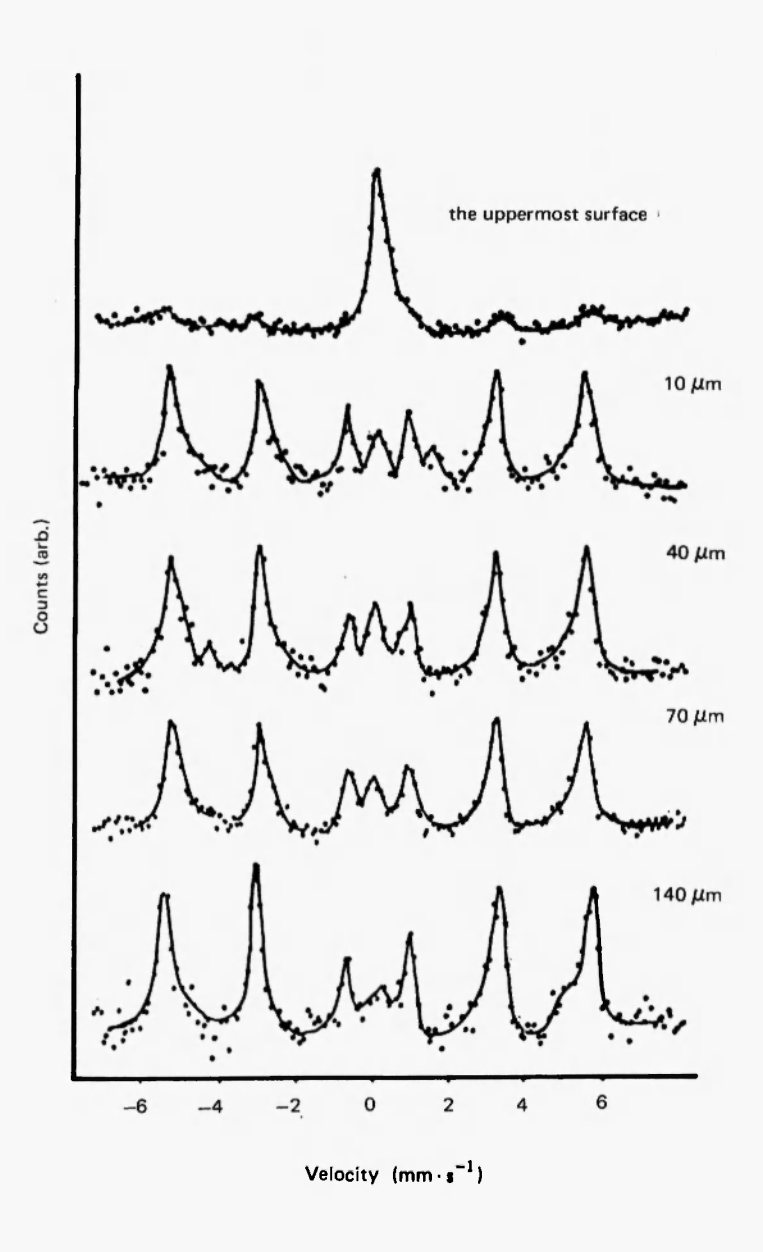
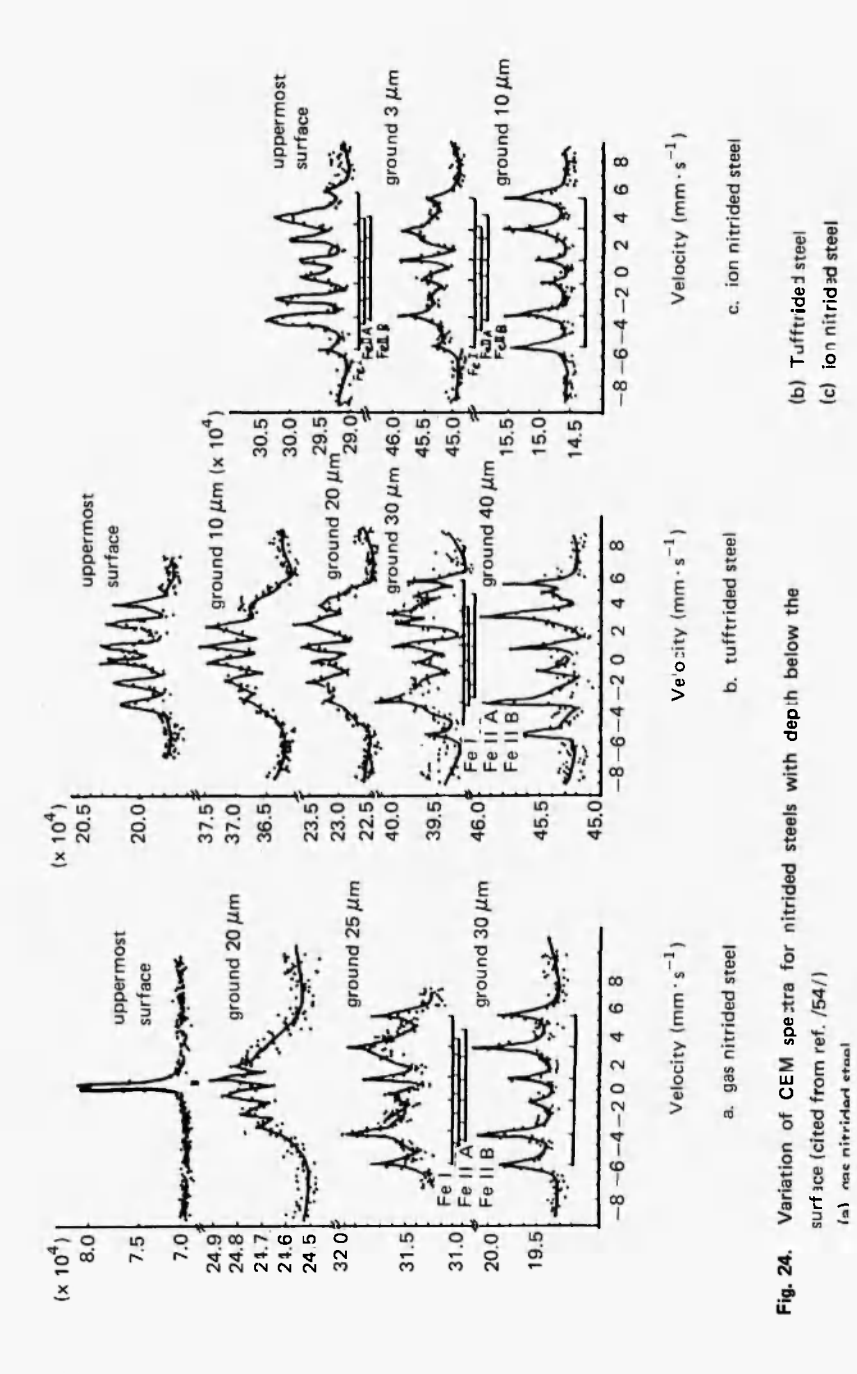


Fig. 23. Variation of CEM spectra of a carburized and quenched steel with depth (cited from ref. /52/)



more than 10 μ m. A Fe_{3+x}N (0 \leq x \leq 1) layer exists between the ϵ -Fe₂N and γ '-Fe₄N layers, the crystal structure of which was distored considerably from that of pure γ '-Fe₄N. The intensity ratio of 3:4:1:1:4:3 of the magnetically split peaks of martensite (γ '-Fe₄N) suggested that the direction of the internal magnetic field of the γ '-Fe₄N layer was parallel to the ground surface and that the layer had undergone the surface effect. The distorted CEM spectrum of the α -Fe layer suggests that the crystal structures of the layer close to γ '-Fe₄N is fairly disturbed by interaction with the γ -Fe₄N layer. The surface layer structure of gas nitrided steel can be illustrated as follows,

$$\begin{vmatrix} (< 10 \,\mu\text{m}) & / & (25 \,\mu\text{m}) & / & / & (30 \,\mu\text{m}) & / \\ \epsilon - \text{Fe}_2 \text{N} & / & \text{distorted} & / & \gamma' - \text{Fe}_4 \text{N} & / & \text{disturbed} & / & \alpha - \text{Fe} \\ & / & \text{Fe}_{3+x} \text{N} & / & / & \alpha - \text{Fe} & / & (\text{substrate}) \end{vmatrix}$$
surface

The multi-layer structure of Tufftrided steel surface, nitrided by dipping the steel into a fused salt bath of potassium cyanide and potassium cyanite for 7 hours, is revealed also by CEM spectrometric observation. The peaks of both ϵ -Fe₃C and ϵ -Fe₃N are seen in Fig. 24(b). This suggests the incorporation of a carbon atom into the ϵ -Fe_{2 \sim 3}N layer. The structure of the Tufftrided steel surface is presented as follows.

$$\epsilon$$
-Fe₃C /intermediate / γ '-Fe₄N /disturbed / α -Fe
 ϵ -Fe₃N / phase / / α -Fe / (substrate)

The surface structure of ion nitrided steel, prepared by placing the steel in a stream of nitrogen (0.35 ℓ/min .) and hydrogen (0.5 ℓ/min .) mixture and ion nitriding for 4 hours at 793 K by the glow discharge of nitrogen, consisted of 3 layers.

Analysis of the CEM spectra, Fig. 24(c), suggests the following layer structure for ion nitrided steel.

Because the relative intensities of the magnetically split γ_1 -Fe₄N peaks, seen in Fig. 24(c), are 3:2:1:1:2:3, the magnetic domain of the uppermost 10 \sim 100 nm layer is supposed to orient at random, suggesting the evaporation of iron atoms by the impact of nitrogen ions, the reaction of iron and nitrogen in the gas phase and sputtering of γ_1 -Fe₄N onto the steel surface.

When 100 keV N_{2}^{+} implants more than $2\times10^{17}~N_{2}~cm^{-2}$ into 125 μ m iron foil, formation of γ -Fe₄N (H; 22.0 T) is recognized at the surface /55/. At $4\times10^{17}~N_{2}~cm^{-2}$, both peaks of γ -Fe₄N and paramagnetic ζ -Fe_{2+x}N (Q.S.: 0.33 mm·s⁻¹) appear. Slightly quadrupole split peaks predominate as the implanted dose of nitrogen increased as shown in Fig. 25. The ζ -Fe_{2+x}N produced by ion implantation is transformed to γ -Fe₄N by treatment at 275°C. A variation in the transformed products with annealing temperature was revealed by analysis of the CEM spectra.

7.6. Characterization of Intermetallic Compounds Formed at the Interface of Coated Metal and Steel

The NRC group in Canada studied the variation of iron-zinc intermetallic compounds produced at a zinc coated steel surface as a function of depth /56/. The steel was galvanised by dipping it in an Fe(0.03%)-Pb(0.5%)-Zn(99.5%) fused solution at 455°C for an hour.

The CEM spectrum of the exposed intermetallic layer of Fe and Zn were observed after mechanically polishing the desired thickness off the surface. It was found that the Zn/Fe ratio decreased with depth depositing discrete intermetallic compounds ζ' , δ - and Γ -phases. A series of CEM spectra, shown in Fig. 26, confirmed the multi-layer structure of the galvanised steel surface as follows.

surface

The variation of intermetallic compounds, formed at the interface of electrotylically plated 90 nm thick tin film and steel by thermal

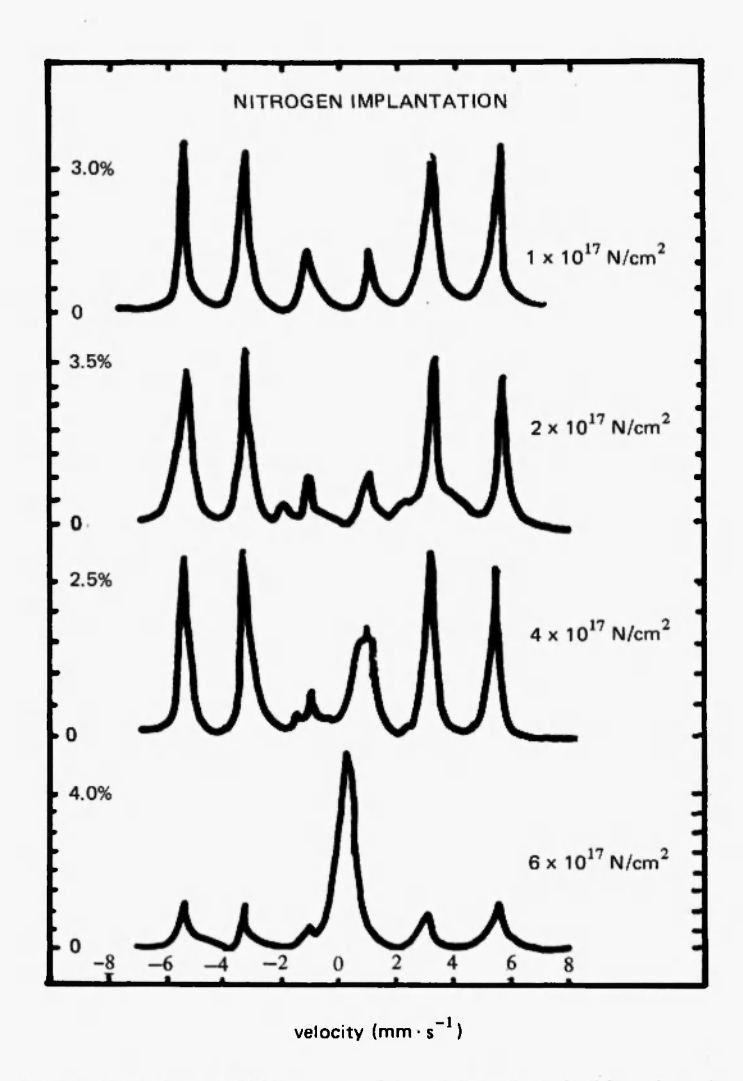


Fig. 25. Variation of CEM spectra of iron foil implanted with various doses of nitrogen (cited from ref. /55/)

treatment up to 700°C for 30 minutes, has been investigated by CEMS /57/. Although no alloy layer is produced by heating at 200°C a FeSn₂ layer begins to deposit at 300°C. As seen in the CEM spectra, Fig. 27, both FeSn₂ and FeSn layers are formed at 400°C, but only FeSn is produced as 500°C. Iron compounds, having I.S. = 0.38 mm·s⁻¹

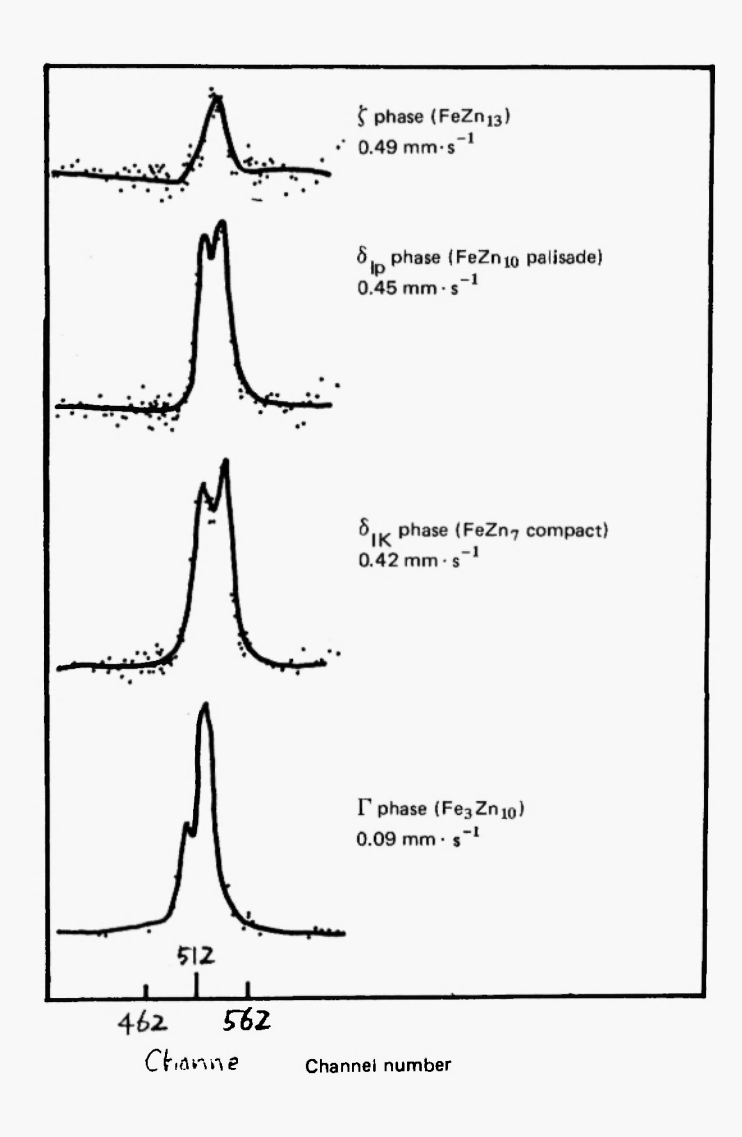
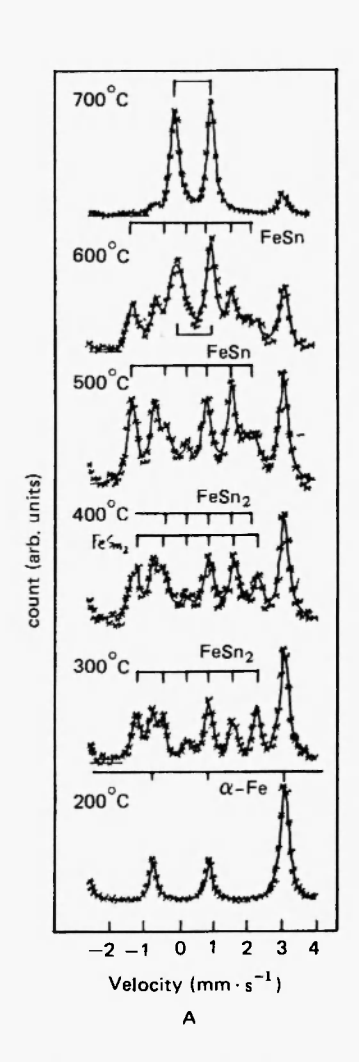


Fig. 26. Variation of CEM spectra with depth for Fe-Zn intermetallic phases formed at a galvanized steel surface (cited from ref. /56/)

and Q.S. = $1.04 \text{ mm} \cdot \text{s}^{-1}$ and assigned to Fe₃ SnC, are deposited at the surface when the tin coated steel is heated at 700° C.



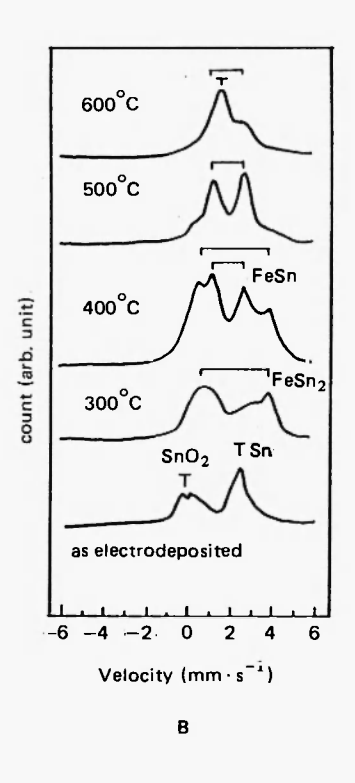


Fig. 27. ⁵⁷Fe and ¹¹⁹Sn CEM spectra of the Fe-Sn intermetallic phase formed by heating tin-plated steel to various temperatures for 30 minutes (cited from ref. /57/)

7.7. STUDY OF PHASE TRANSFORMATION

Evidence that an increase in austenite improves the fracture toughness of Fe-9Ni-0.1C steel was revealed by means of XMS, which

also confirmed the transformation of the austenite present within the 300 μ m layer of the surface to martensite after the fracture of the steel at 77 K /58/. The transformation of the retained austenite (5 ~ 10%) to martensite in the ductile fracture surface of grain-refined 9Ni-Fe cryogenic steel was also shown by the application of CEMS /59/. Although the austenite peak was not seen in the CEM spectrum of the freshly fractured surface and electrolytic etching of the surface to a depth of 0.1 mm did not cause any change in the spectrum, the singlet peak due to austenite appeared after the removal of the surface layer by etching to 1 mm (Fig. 28). This result suggests that the transformation of retained austenite to martensite is compatible with the low temperature toughness of steel.

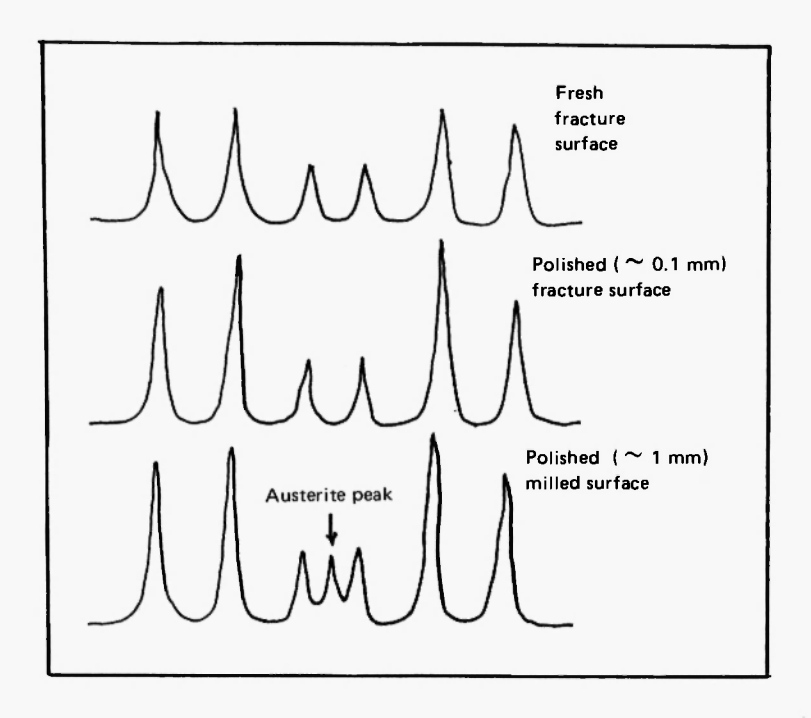


Fig. 28. CEM spectra of the fractured surface of grain-refined cryogenic steel broken at 77 K (cited from ref. /59/)

7.8 STUDY OF CRYSTALLIZATION OF AMORPHOUS IRON

A distinctive feature of Mössbauer spectrometry is that it is applicable to amorphous as well as crystalline materials. This has been used for the observation of the crystallization behavior of amorphous iron-Fe_{80 5}Si_{4 0}B₁₂C₃ /60/. Quatenary amorphous iron ribbon 25 mm wide and 35 µm thick was annealed in N2-H2 at 590°C for 1 hour and both transmission and conversion electron Mössbauer spectra were observed to identify the compounds deposited on crystallization /61/. TM and CEM spectra give information on the bulk and surface region, respectively. Analyses of the TM and CEM spectra for the thermally treated Fe_{80.5} S_{4.0} B₁₂C₃, shown in Fig. 29, revealed that magnetic orientation of the amorphous phase in the bulk changes when heating to 435 ~ 450°C, since the intensity of the second peak diminishes remarkably. On the other hand, the magnetic orientation of the surface layer does not change - parallel to the surface plain since the intensity of the second peak remains unchanged. The sharpness of the peak is a good measure of crystallinity. Fig. 29 suggests that crystallization proceeds more easily at the surface than in the bulk.

7.9 CEMS FOR 119Sn AND 181Ta

Other nuclides which have been studied by CEMS are ¹¹⁹Sn, ¹⁵¹Eu, ¹⁶⁹Tm and ¹⁸¹Ta. The radiations emitted by these nuclei are shown in Table 6. The excitation and de-excitation processes for the ¹¹⁹Sn nucleus following the absorption of resonant 23.8 keV γ -ray are illustrated in Fig. 30. 84% of excited ^{119m}Sn (I; 3/2 –) nuclei reemit 19.6 keV L-conversion electrons, followed by radiation of 2.8 keV LMM-Auger electrons. The range of the 19.6 keV electron is estimated to be 30 nm \sim 1 μ m in metallic tin /62/. The 23.8 keV γ ray is incident onto the tin sample from a 15 mCi ^{119m}Sn source of BaSnO₃ (1 mCi = 3.7 × 10⁷ Bq) through a 25.4 μ m Pd filter, which reduces the K $_{\alpha}$ and K $_{\beta}$ X rays of Sn (25.0 and 25.3 keV, respectively).

The CEM spectra of 119 Sn for iron plated with 0.336 mg/cm² tin, heat-treated at 290 $\sim 310^{\circ}$ C and cooled down by passage through water, are shown in Fig. 31. Peaks due to Sn, SnO₂ and Fe-Sn₂ are seen in the spectrum /10/.

The production of an alloy layer between tin and iron by heat treatment was studied for 90 nm tin plated steel /56/. The ¹¹⁹Sn-CEM

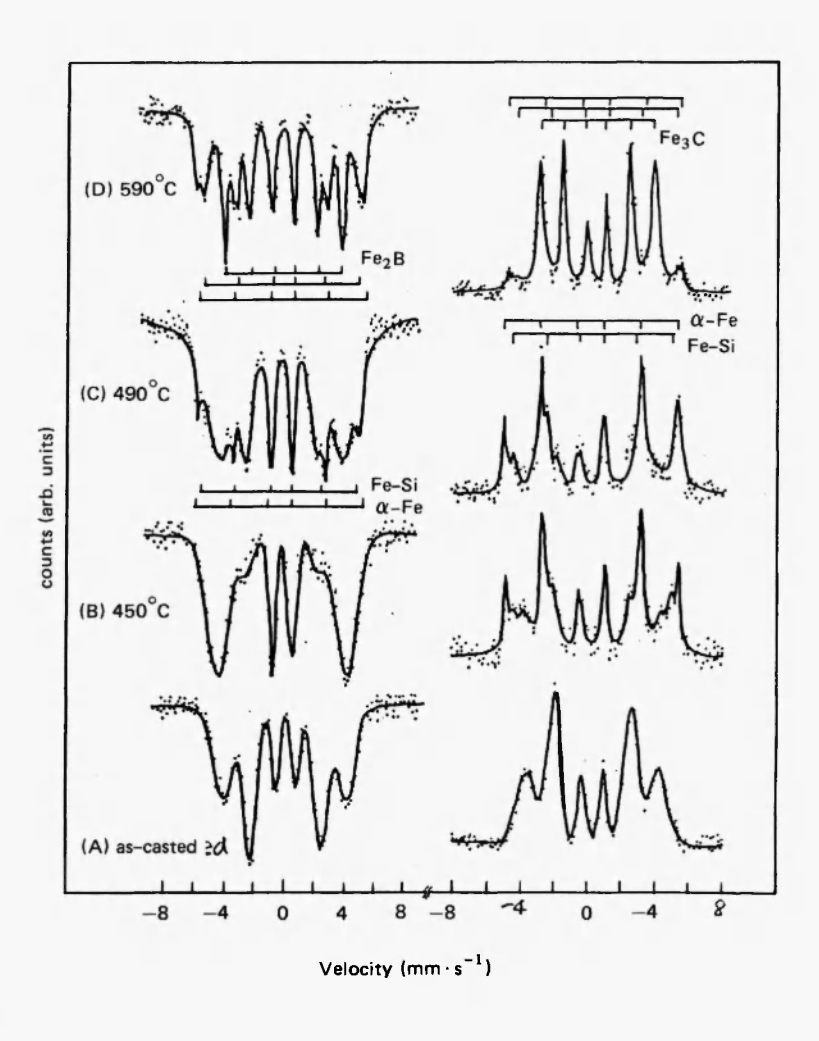


Fig. 29. TM and CEM spectra observed for the bulk and surface regions of amorphous iron (Fe_{80.5}B₁₂Si_{4.5}C₃) prepared by the single roler quenching method

spectra (Fig. 27B) reveal that alloys of different composition are deposited by thermal treatment at different temperatures. The result coincides with that obtained by ⁵⁷Fe CEMS as described in Section 7.6.

TABLE 6
Ranges of radiations reemitted from excited ¹¹⁹Sn, ¹⁵¹Eu, ¹⁶⁹Tm and ¹⁸¹Ta nuclei

nucleus (transition)	source (half life)	reemitted radiation	energy (keV)	probability	range in metal (nm)
		γ гау	23.8	16%	1 × 10 ⁶
¹¹⁹ Sn	119mSn	L conversion electron	19.6	86%	$30 \sim 5 \times 10^4$
(23.8 keV)	(250 d)	M conversion electron	23.0	13%	$30 \sim 7 \times 10^4$
		LMM Auger electron	2.8	75%	5 ~ 50
¹⁵¹ Eu	¹⁵¹ Sm	L conversion electron	13.5		
(21.6 keV)	(88 y)	K _{Q1} X ray	41.5		
¹⁶⁹ Tm	¹⁶⁹ Er	M conversion electron	6.1		
(8.4 keV)	(9.4 d)	K _{α1} X ray	50.7		
¹⁸¹ Ta	¹⁸¹ W	γгау	6.2		
		M conversion electron	3.5	33%	33
(6.2 keV)	(121 d)	K _{O1} X ray	57.6		

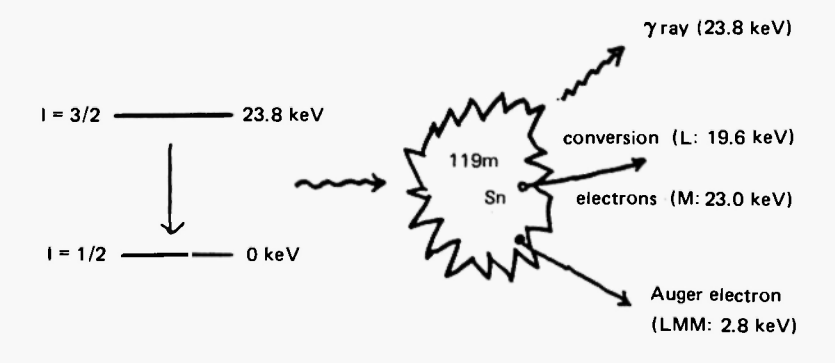


Fig. 30. Resonant absorption of 23.8 keV γ rays by the ¹¹⁹Sn (I = 1/2) nucleus and radiations from the excited ^{119m}Sn (I = 3/2) nucleus

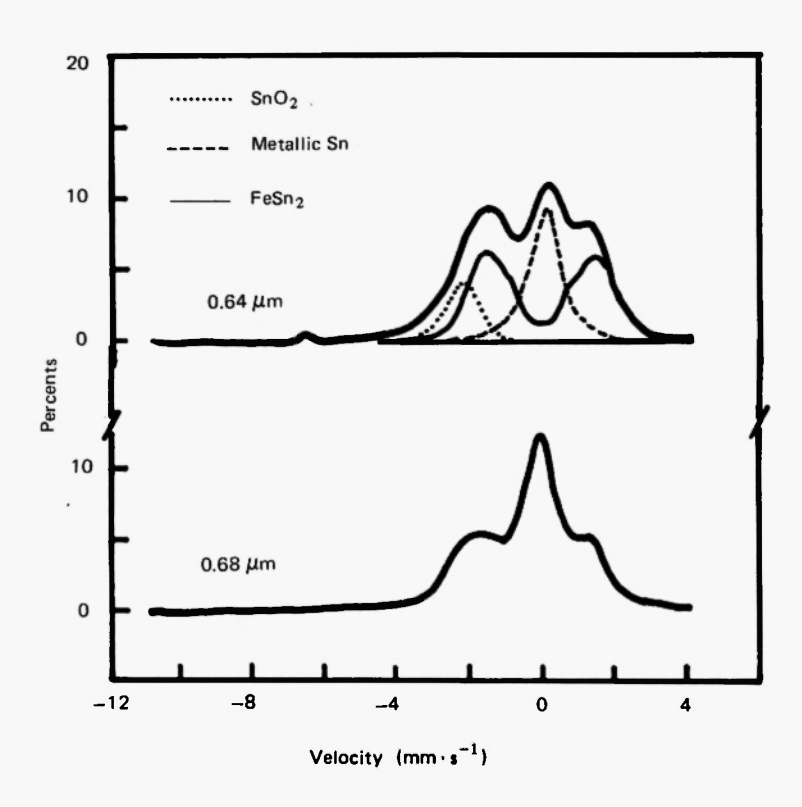


Fig. 31. 119 Sn CEM spectra of tin-plated steel (cited from ref. /10/). Peaks are attributed to FeSn₂, Sn, and SnO₂ upper (Sn thickness: 0.46 μ m)

lower (Sn thickness: 0.68 µm)

Corrosion studies of tin and tin-coated iron have also been reported /63/. H_2SnO_3 (meta-stannic acid) was produced by immersion of tin plate in 1 M HNO₃ for 5 minutes and $Sn_2P_2O_7$ (stannic pyrophosphate) was formed by dipping the same sample in 2 M H_3PO_4 for 5 days.

CEM spectra arising from the 3.5 keV conversion electron reemitted from the 181 Ta nucleus have been reported. The practical range of the 3.5 keV electron was estimated to be approximately 55 μ m/cm² or 33 nm in Ta metal. The somewhat broader peak and I.S. obtained for Ta foil suggested absorption of gases at the Ta surface /11/.

ACKNOWLEDGEMENT

The author wishes to express his gratitude to Prof. Atsushi Mizuike, Nagoya University, for encouragement and helpful discussion during the preparation of this manuscript.

REFERENCES

- GREENWOOD, N.N. and GRIBB, T.C., "Mössbauer Spectroscopy", Chapman and Hall, London (1971).
- GONSER, U., Ed., "Mössbauer Spectroscopy" (Topics in Applied Physics 5), Springer-Verlag, Berlin (1975).
- COHEN, R.L., Ed., "Applications of Mössbauer Spectroscopy", Vols. 1 and 2, Academic Press, London (1976 and 1980).
- VERTES, A., KORECZ, L. and BURGER, K., "Mössbauer Spectroscopy" (Studies in Physical and Theoretical Chemistry 5), Elsevier Sci. Publ., Amsterdam (1979).
- SHENOY, G.K. and WAGNER, F.E., Eds., "Mössbauer Isomer Shifts", North-Holland Publ., Amsterdam (1978).
- SPIJKERMAN, J.J., in GRUVERMAN, I.J., Ed., "Mössbauer Effect Methodology", Vol. 7, Plenum Press, New York, pp. 85-96 (1971).
- 7. UJIHIRA, Y. and NOMURA, K., Bunseki, 555 (1978).
- 8. BERRY, F.J., Transition Met. Chem., 4, 209 (1979).
- STEVENS, J.G., STEVENS, V.E., WHITE, R.M. and GIBSON, J., Eds., "Conversion Electron Mössbauer Spectroscopy" (Mössbauer Handbook), Mössbauer Effect Data Center, Univ. of North Carolina, Ashville, U.S.A. (1982).
- HUFFMAN, G.P. and DUNMYRE, G.R., J. Electrochem. Soc., 125, 1652 (1978).
- SALOMON, D., WEST, P.J. and WEYER, G., Hyperfine Interactions, 5, 61 (1977).
- 12. SIMONS, G.W. and LEIDHEISER, H., Jr., Characterization of Metal and Polymer Surfaces (symposium), 49 (1977).
- 13. HUFFMAN, G.P. and PODGURSKI, H.H., Oxidation Metals, 10, 377 (1976).
- 14. MOSSBAUER, R.L., Z. Physik, 151, 124 (1958).
- 15. FUJIO, Y., Jap. J. Appl. Phys., 12, 1850 (1973).
- 16. KEISCH, B., J. de Phys., 35, C6-151 (1974).
- KEISCH, B., in COHEN, R.L., Ed., "Application of Mössbauer Spectroscopy", Vol. 1, Academic Press, pp. 263-286 (1967).
- 18. SWANSON, K.R. and SPIJKERMAN, J.J., J. Appl. Phys., 41, 3155 (1970).
- COLLINS, R.L., MAZAK, R.A. and YAGNIK, C.M., in "Mössbauer Effect Methodology", Vol. 8, p. 191 (1973).

- TORIYAMA, T., SANEYOSHI, K. and HISATAKE, K., J. de Phys.,
 40, C2-14 (1979).
- 21. BAVERSTAM, U., BODLUND-RINGSTOM, B., BOHN, C., EKDAHL, T. and LILJEQUIST, D., Nucl. Instr. Methods, 154, 401 (1978).
- PARELLADA, J., POLCARI, M.R., BURIN, K. and ROTHBERG, G.M., Nucl. Instr. Methods, 179, 113 (1981).
- 23. YANG, T., TROOSTER, J., KACHNOWSKI, T. and KOLLAR, N.B., Hyperfine Interaction. 10, 795 (1981).
- BOKEMEYER, H., WAHLFAHRT, K., KANKELEIT, E. and ECKARDT,
 D., Z. Physik, A.274, 304 (1975).
- NAKAGAWA, H., NOMURA, K. and UJIHIRA, Y., Radioisotopes, 31, 94 (1982).
- 26. MASSENET, O. and DAVER, H., Sol. Stat. Comm., 25, 917 (1978).
- MASSENET, O., COEY, J.M.D. and CHAPPERT, J., Nucl. Instr. Methods, 161, 83 (1979).
- HANDA, A., KOBAYASHI, J. and UJIHIRA, Y., Appl. Surf. Sci., submitted.
- LILJEQUIST, D. and BODLUNG-RINGSTOM, B., Nucl. Instr. Methods, 160, 131 (1979).
- 30. PROYKOVA, A., Nucl. Instr. Methods, 160, 321 (1979).
- BAVERSTAM, M., EKDAHL, T., BOHM, C., LILJEQUIST, D. and RING-STOM, B., Nucl. Instr. Methods, 118, 313 (1974).
- NAKAGAWA, H., UJIHIRA, Y. and INABA, M., Nucl. Instr. Methods, 196, 573 (1982).
- 33. THOMAS, J.M., TRICKER, M.J. and WINTERBOTTOM, A.P., J. Chem. Soc., Faraday Trans., 1975, 1708.
- SHIGEMATSU, T., PFANNES, H.D. and KEUNE, W., Phys. Rev. Letters, 45, 1206 (1980).
- SWANSON, K.R. and SPIJKERMAN, J.J., J. Appl. Phys., 41, 3155 (1970).
- ENSLING, J., FREISCH, J., GRIMM, R., GRÜBER, J. and GÜTLICH, P., Corrosion Science, 18, 797 (1978).
- 37. UJIHIRA, Y. and NOMURA, K., Japan Analyst, 27, 782 (1978).
- RAMSHESH, V., RAVICHANDRAN, K. and VENKATESWARLE, K.S., Indian J. Chem., 20A, 867 (1981).
- 39. FUJINAMI, M. and UJIHIRA, Y., Appl. Surf. Sci., 17, 265 (1984).
- 40. FUJINAMI, M. and UJIHIRA, Y., Appl. Surf. Sci., 17, 276 (1984).
- 41. BERRY, F.J., J. Chem. Soc., Dalton Trans., 1979, 1736.
- 42. UJIHIRA, Y. and NOMURA, K., J. de Phys., 41, C1-391 (1980).
- 43. NOMURA, K. and UJIHIRA, Y., Nippon Kagakukaishi, 1982, 1352.
- 44. NOMURA, K. and UJIHIRA, Y., J. Mater. Sci., 17, 3437 (1982).
- NOMURA, K., UJIHIRA, Y., MATSUSHITA, Y., ROJIMA, R. and SUGA-HARA, Y., Nippon Kagakukaishi, 1980, 1372.

- NOMURA, K., UJIHIRA, Y. and KOJIMA, R., Nippon Kagakukaishi, 1982, 87 (1982).
- NOMURA, K., UJIHIRA, Y. and KOJIMA, R., Nippon Kagakukaishi, 1982, 791 (1982).
- 48. NOMURA, K. and UJIHIRA, Y., J. Anal. Appl. Pyrolysis, 5, 221 (1983).
- 49. NOMURA, K. and UJIHIRA, Y., J. Mater. Sci., 18, 1751 (1983).
- 50. HANDA, A. and UJIHIRA, Y., J. Mater. Sci., 18, 1787 (1983).
- CARBUCICCHIO, M., BARDANI, L. and PALOMBARINI, G., J. Mater. Sci., 15, 711 (1980).
- 52. HANDA, A., UJIHIRA, Y. and OKABE, I., J. Mater. Sci., 16, 1999 (1981).
- 53. UJIHIRA, Y. and HANDA, A., J. de Phys., 40, C2-586 (1979).
- UJIHIRA, Y., HANDA, A., ABE, Y. and OKABE, I., Nippon Kagakukaishi, 1979, 234.
- LONGWORTH, G. and HARTLEY, N.E.W., Thin Solid Films, 48, 95 (1978).
- GRAHAM, M.J., BEAUBIEN, P.E. and SPROULE, G.L., J. Mater. Sci., 15, 626 (1980).
- UJIHIRA, Y., FUJINAMI, M., YOSHIDA, K. and TERASAKA, M., J. Mater. Sci., in press.
- 58. KIM, K.J. and SCHWARTZ, L.H., J. de Phys., 37, C6-406 (1979).
- SYN, C.K., FULTZ, B. and MORRIS, J.W., Jr., Metallurgical Trans., 9A, 1635 (1978).
- 60. SAEGUSA, N. and MORRISH, A.H., Phys. Rev. B, 22, 3472 (1980).
- 61. FUJINAMI, M. and UJIHIRA, Y., J. Non-Crystal. Solids, in press.
- YAGNIK, C.M., MAZAK, R.A. and COLLINS, R.L., Nucl. Insterum. Methods, 114, 1 (1974).
- ENDO, K., SHIBUYA, M. and SANO, H., Radiochem., Radioanal. Letters, 28, 363 (1977).